Does ribosome composition maximize growth rate? The role of RNA instability

Diana Széliová[1*†], **Stefan Müller**[2*†], **Jürgen Zanghellini**[1*†]

[1]Department of Analytical Chemistry, University of Vienna, Austria, EU; [2]Faculty of Mathematics, University of Vienna, Austria, EU

***For correspondence:**
diana.szeliova@univie.ac.at (DZ);
st.mueller@univie.ac.at (SM);
juergen.zanghellini@univie.ac.at (JZ)

[†]All authors contributed equally to this work

Abstract Ribosomes are protein synthesis machines that are central to cellular self-fabrication, and the synthesis time of a ribosome places an upper bound on growth rate. While most cellular enzymes are proteins, ribosomes consist of 1/3 protein and 2/3 RNA (in *E. coli*). Recent research suggests that ribosome composition arises from a trade-off between two "autocatalytic loops", ribosomal protein and RNA polymerase synthesis, respectively.

In this work, we develop a (coarse-grained) mechanistic model of a self-fabricating cell, validate it under different growth conditions, and use resource balance analysis (RBA) to study maximum growth rate as a function of ribosome composition. Our model highlights the importance of RNA instability. If we neglect it, RNA synthesis is always "cheaper" than protein synthesis, leading to an RNA-only ribosome at maximum growth rate.

To account for RNA turnover, we explore two scenarios regarding the activity of RNases. In (a) degradation is proportional to RNA content, whereas in (b) ribosomal proteins cooperatively mitigate RNA instability by protecting it from misfolding and subsequent degradation. In both cases, an increase in ribosomal protein content raises protein synthesis costs while reducing RNA turnover costs. This leads to a mixed ribosome composed of RNA and proteins. However, only in scenario (b), where we consider the cooperative protection of ribosomal RNA by proteins, our model predictions are in qualitative agreement with experimental data under different growth conditions.

Our research offers new mechanistic insights into ribosome biogenesis and evolution. Furthermore, it paves the way for understanding the protein-rich ribosome composition found in archaea and mitochondria.

Contents

Introduction

The ribosome is at the core of any (known) self-replicating organism. In a process called translation, ribosomes read the instructions from messenger ribonucleic acids (mRNAs) to synthesize the corresponding proteins, including ribosomal proteins (rPs). This autocatalytic nature of ribosomes ultimately limits the doubling time of a cell to the period it takes a ribosome to synthesize itself (***Dill et al., 2011***; ***Shore and Albert, 2022***). In *E. coli* this would be $6\,\mathrm{min}$, assuming that the ribosome consists of a 55-protein complex of approximately 7400 amino acids (AAs) that is translated at a speed of $21\,\mathrm{AA/sec}$ (***Bremer and Dennis, 1996***). In fact, even in growth-optimized *E. coli*, that doubling limit remains far from being reached (***Long et al., 2017***). Nonetheless, it has been proposed that ribosomes, not only in *E. coli*, have been subjected to strong selective pressure to minimize their own duplication time in order to speed up the production of all other proteins (***Reuveni et al., 2017***). With this principle in mind, ***Reuveni et al.* (*2017*)** explain why ribosomes have many rPs of similar length.

Ribosomes are structures that have developed over time by adding ribosomal ribonucleic acid (rRNA) and rP around a central core (***Petrov et al., 2015***). This core is considered to be a leftover from ancient translation systems that evolved alongside the genetic code. Different types of ribosomes have evolved in bacteria, archaea, and eukaryotes, but their overall structures are similar within each kingdom (***Melnikov et al., 2018***). For example, the mass of ribosomes in prokaryotes is made up of approximately $63\,\%$ rRNA and $37\,\%$ rPs (***Melnikov et al., 2012***; ***Kurland, 1960***), whereas eukaryotic ribosomes have an equal mass distribution of rRNA and rPs (***Wilson and Cate, 2012***; ***Verschoor et al., 1998***; ***Reuveni et al., 2017***). Thus, the question arises whether there is an evolutionary advantage in having such a high ribonucleic acid (RNA) content.

It has been suggested that the ribosome composition can be understood as a competition for resources between rRNA synthesis and rP synthesis (***Kostinski and Reuveni, 2020***; ***Klumpp, 2020***). In particular, ***Kostinski and Reuveni* (*2020*)** derived two upper bounds on growth rate resulting from two "autocatalytic loops", one for rP production, and one for RNA polymerase (RNAP) and rRNA production. By analyzing allocation data from *E. coli*, they concluded that maximum growth rate occurs at the current ribosome composition of 2/3 RNA and 1/3 protein. However, the specific processes that limit the two autocatalytic processes remained elusive.

Here we aim to provide a mechanistic understanding of these processes. We set up a small (coarse-grained) model of a self-replicating cell and perform resource balance analysis (RBA) (***Goelzer et al., 2015***). In particular, we vary ribosome composition *and* "ribosome allocations" (fractions of ribosomes allocated to the synthesis of different proteins) and maximize growth rate.

We find that the costs of stabilizing rRNA strongly influence the optimal ribosome composition. If we neglect rRNA turnover, our predictions suggest the presence of RNA-only ribosomes (in contrast to experimental evidence). Taking RNA degradation into account, increases its biosynthesis costs, and maximum growth occurs for a mixed (RNA+protein) ribosome.

Results

We introduce a (coarse-grained) mechanistic model of a self-fabricating cell and investigate optimal ribosome composition using RBA. That is, we maximize growth rate under several sets of con-

(a)

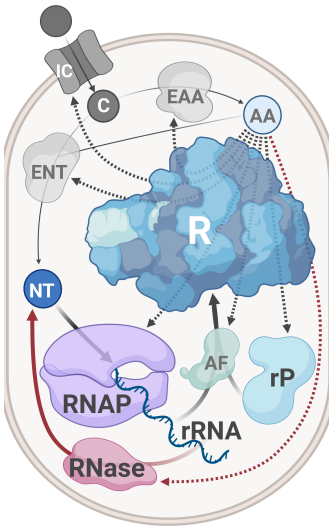

(b)

$$
\begin{array}{c}
 \\
\text{C} \\
\text{AA} \\
\text{NT} \\
\text{rRNA} \\
\text{rP} \\
\text{IC} \\
\text{EAA} \\
\text{ENT} \\
\text{RNAP} \\
\text{RNase} \\
\text{AF} \\
\text{R}
\end{array}
\begin{array}{c}
\begin{array}{ccccccccccccc}
r_{\text{IC}} & r_{\text{EAA}} & r_{\text{ENT}} & r_{\text{RNAP}} & r_{\text{RNase}} & r_{\text{AF}} & s_{\text{IC}} & s_{\text{EAA}} & s_{\text{ENT}} & s_{\text{RNAP}} & s_{\text{RNase}} & s_{\text{AF}} & s_{\text{R}}
\end{array} \\
\begin{pmatrix}
1 & -n_{\text{AA}} & -n_{\text{NT}} & 0 & 0 & 0 & 0 & 0 & 0 & 0 & 0 & 0 & 0 \\
0 & 1 & -1 & 0 & 0 & 0 & -n_{\text{IC}} & -n_{\text{EAA}} & -n_{\text{ENT}} & -n_{\text{RNAP}} & -n_{\text{RNase}} & -n_{\text{AF}} & -n_{\text{rP}} \\
0 & 0 & 1 & -n_{\text{rRNA}} & n_{\text{rRNA}} & 0 & 0 & 0 & 0 & 0 & 0 & 0 & 0 \\
0 & 0 & 0 & 1 & -1 & -1 & 0 & 0 & 0 & 0 & 0 & 0 & 0 \\
0 & 0 & 0 & 0 & 0 & -1 & 0 & 0 & 0 & 0 & 0 & 0 & 1 \\
0 & 0 & 0 & 0 & 0 & 0 & 1 & 0 & 0 & 0 & 0 & 0 & 0 \\
0 & 0 & 0 & 0 & 0 & 0 & 0 & 1 & 0 & 0 & 0 & 0 & 0 \\
0 & 0 & 0 & 0 & 0 & 0 & 0 & 0 & 1 & 0 & 0 & 0 & 0 \\
0 & 0 & 0 & 0 & 0 & 0 & 0 & 0 & 0 & 1 & 0 & 0 & 0 \\
0 & 0 & 0 & 0 & 0 & 0 & 0 & 0 & 0 & 0 & 1 & 0 & 0 \\
0 & 0 & 0 & 0 & 0 & 0 & 0 & 0 & 0 & 0 & 0 & 1 & 0 \\
0 & 0 & 0 & 0 & 0 & 1 & 0 & 0 & 0 & 0 & 0 & 0 & 0
\end{pmatrix}
\end{array}
= \boldsymbol{N}
$$

$$
\begin{pmatrix} v_{\text{IC}}, & v_{\text{EAA}}, & v_{\text{ENT}}, & v_{\text{RNAP}}, & v_{\text{RNase}}, & v_{\text{AF}}, & w_{\text{IC}}, & w_{\text{EAA}}, & w_{\text{ENT}}, & w_{\text{RNAP}}, & w_{\text{RNase}}, & w_{\text{AF}}, & w_{\text{rP}} \end{pmatrix} = \boldsymbol{v}^T
$$

Figure 1. A small model of a self-fabricating cell. (a) The cell imports a carbon source (C) and has two types of metabolic enzymes synthesizing amino acids (AA) from the carbon source and nucleotides (NT) from the carbon source and amino acids. The RNA polymerase (RNAP) uses nucleotides to form the ribosomal RNA (rRNA), and the ribosome (R) uses amino acids to synthesize the importer (IC), the metabolic enzymes (EAA, ENT), the ribosomal assembly factors (AF), and the ribosomal protein (rP). Finally, the assembly factors build the ribosome from ribosomal RNA and protein. The processes above constitute the base model. In the extended model, RNase degrades ribosomal RNA (and is synthesized by the ribosome). The additional processes are shown in red. **(b)** The resulting stoichiometric matrix and the corresponding flux vector. Here, s is used for protein *synthesis* reactions (and w for the corresponding fluxes), and r is used for all other reactions (and v for the corresponding fluxes). Additional columns and rows for the extended model are shown in red.

straints. We validate the model by predicting RNAP fluxes and RNA to protein ratios at different growth rates. Ultimately, we predict maximum growth rate at different ribosome compositions.

A small model of a self-fabricating cell

We consider the small (coarse-grained) model of a self-fabricating cell depicted in ***Figure 1***. The cell imports a carbon source (C) and has two types of metabolic enzymes, one synthesizing amino acids (AA) from the carbon source and the other one synthesizing nucleotides (NT) from the carbon source and amino acids. RNA polymerase (RNAP) uses nucleotides to form the ribosomal RNA (rRNA), while the ribosome (R) uses amino acids to synthesize all proteins, including the importer (IC), the metabolic enzymes (EAA, ENT), the RNA polymerase and optionally a ribonuclease (RNase), the ribosomal assembly factors (AF), and the ribosomal proteins (rP). Finally, the assembly factors build the ribosome from ribosomal RNA and protein. In a base model, we neglect RNA degradation, whereas in an extended model we consider the enzyme (RNase) that breaks down RNA into nucleotides. We now provide a more formal definition of the two models.

Given the stoichiometric matrix $\boldsymbol{N}$ and the vector of molar masses $\boldsymbol{\omega}$, the dynamic model of cellular growth relates growth rate μ, the vector of (metabolite, RNA, protein, and ribosome) concentrations $\boldsymbol{c}$, and the vector of fluxes ($\boldsymbol{v}$ for "enzymatic" reactions and $\boldsymbol{w}$ for protein synthesis) according to

$$
\frac{\mathrm{d}\boldsymbol{c}}{\mathrm{d}t} = \boldsymbol{N}\begin{pmatrix}\boldsymbol{v}\\ \boldsymbol{w}\end{pmatrix} - \mu\,\boldsymbol{c} \qquad \text{and} \qquad \boldsymbol{\omega}^T\boldsymbol{c} = 1.
$$

At steady state, growth rate μ and concentrations $\boldsymbol{c}$ are determined by the fluxes $\boldsymbol{v}$ and $\boldsymbol{w}$,

$$
\boldsymbol{N}\begin{pmatrix}\boldsymbol{v}\\ \boldsymbol{w}\end{pmatrix} = \mu\,\boldsymbol{c} \geq \boldsymbol{0} \qquad \text{and} \qquad \mu = \boldsymbol{\omega}^T\boldsymbol{N}\begin{pmatrix}\boldsymbol{v}\\ \boldsymbol{w}\end{pmatrix}. \tag{1}
$$

Table 1. Constraints used in the "extended" and "base" models (with and without RNA degradation), see ***Figure 1***. In particular, stoichiometric constraints (for the "metabolites" C, AA, NT, rRNA, rP), capacity constraints (for the catalysts IC, EAA, ENT, RNAP, RNase, AF, R), and the (dry) mass constraint. The column 'sign' indicates an equality (=) or inequality (≥) constraint, and the column 'rhs' specifies the right-hand side (a homogeneous or inhomogeneous constraint). Additional columns and rows for the extended model are shown in red.

	v_{IC}	v_{EAA}	v_{ENT}	v_{RNAP}	v_{RNase}	v_{AF}	w_{IC}	w_{EAA}	w_{ENT}	w_{RNAP}	w_{RNase}	w_{AF}	w_{rP}	sign	rhs
C	1	$-n_{\mathrm{AA}}$	$-n_{\mathrm{NT}}$	0	0	0	0	0	0	0	0	0	0	=	0
AA	0	1	-1	0	0	0	$-n_{\mathrm{IC}}$	$-n_{\mathrm{EAA}}$	$-n_{\mathrm{ENT}}$	$-n_{\mathrm{RNAP}}$	$-n_{\mathrm{RNase}}$	$-n_{\mathrm{AF}}$	$-n_{\mathrm{rP}}$	=	0
NT	0	0	1	$-n_{\mathrm{rRNA}}$	n_{rRNA}	0	0	0	0	0	0	0	0	=	0
rRNA	0	0	0	1	-1	-1	0	0	0	0	0	0	0	≥ (=)	0
rP	0	0	0	0	0	-1	0	0	0	0	0	0	1	≥	0
cap IC	$-\mu$	0	0	0	0	0	$k_{\mathrm{IC}}^{\mathrm{cat}}$	0	0	0	0	0	0	≥	0
cap EAA	0	$-\mu$	0	0	0	0	0	$k_{\mathrm{EAA}}^{\mathrm{cat}}$	0	0	0	0	0	≥	0
cap ENT	0	0	$-\mu$	0	0	0	0	0	$k_{\mathrm{ENT}}^{\mathrm{cat}}$	0	0	0	0	≥	0
cap RNAP	0	0	0	$-\mu n_{\mathrm{rRNA}}$	0	0	0	0	0	$\bar{k}_{\mathrm{RNAP}}^{\mathrm{el}}$	0	0	0	≥	0
cap RNase	0	0	0	0	$-\mu n_{\mathrm{rRNA}}$	0	0	0	0	0	$k_{\mathrm{RNase}}^{\mathrm{deg}}$	0	0	≥	0
cap AF	0	0	0	0	0	$-\mu$	0	0	0	0	0	$k_{\mathrm{AF}}^{\mathrm{cat}}$	0	≥	0
cap R	0	0	0	0	0	$\bar{k}_{\mathrm{R}}^{\mathrm{el}}$	$-\mu n_{\mathrm{IC}}$	$-\mu n_{\mathrm{EAA}}$	$-\mu n_{\mathrm{ENT}}$	$-\mu n_{\mathrm{RNAP}}$	$-\mu n_{\mathrm{RNase}}$	$-\mu n_{\mathrm{AF}}$	$-\mu n_{\mathrm{rP}}$	≥ (=)	0
min deg	0	0	0	0	μ	$-k^{\mathrm{deg}}(1-x_{\mathrm{rP}})$	0	0	0	0	0	0	0	≥ (=)	0
(dry) mass	ω_{C}	0	0	0	0	0	0	0	0	0	0	0	0	=	μ

To take limited cellular resources into account, we consider capacity constraints for the "enzymatic" fluxes $\boldsymbol{v}$, including transcription (and optionally RNA degradation),

$$v_i \le k_i^{\mathrm{cat}} c_i, \quad i \in \{\mathrm{IC}, \mathrm{EAA}, \mathrm{ENT}, \mathrm{AF}\}, \tag{2a}$$

$$n_{\mathrm{rRNA}} v_{\mathrm{RNAP}} \le \bar{k}_{\mathrm{RNAP}}^{\mathrm{el}} c_{\mathrm{RNAP}}, \tag{2b}$$

$$(n_{\mathrm{rRNA}} v_{\mathrm{RNase}} \le k_{\mathrm{RNase}}^{\mathrm{deg}} c_{\mathrm{RNase}}). \tag{2c}$$

Further, we consider the ribosome capacity constraint for the protein fluxes $\boldsymbol{w}$,

$$\sum_{i \in \mathrm{Proteins}} n_i w_i \le \bar{k}_{\mathrm{R}}^{\mathrm{el}} c_{\mathrm{R}}, \quad \mathrm{Proteins} = \{\mathrm{IC}, \mathrm{EAA}, \mathrm{ENT}, \mathrm{RNAP}, (\mathrm{RNase}), \mathrm{AF}, \mathrm{rP}\}. \tag{2d}$$

Here, n_{rRNA} is the number of nucleotides in rRNA, n_i is the number of amino acids in protein i, k_i^{cat} is the corresponding enzyme turnover rate, and $\bar{k}_{\mathrm{RNAP}}^{\mathrm{el}} = k_{\mathrm{RNAP}}^{\mathrm{el}} f_{\mathrm{RNAP}}^{\mathrm{act}}$ and $\bar{k}_{\mathrm{R}}^{\mathrm{el}} = k_{\mathrm{R}}^{\mathrm{el}} f_{\mathrm{R}}^{\mathrm{act}}$ are the effective transcription and translation elongation rates, respectively. As mentioned above, RNase is synthesized optionally and hence put in brackets. By defining the "ribosome allocations",

$$\phi_i^{\mathrm{R}} = \frac{n_i w_i}{\bar{k}_{\mathrm{R}}^{\mathrm{el}} c_{\mathrm{R}}}, \quad i \in \mathrm{Proteins}, \tag{3}$$

that is, the fraction of ribosomes translating a certain protein i, constraint (2d) can be written as

$$\sum_{i \in \mathrm{Proteins}} \phi_i^{\mathrm{R}} \le 1.$$

We refer to the model given by Equations (1) and (2abd) as the *base* RBA model. Equations (1) and (2), including (2c), define the *extended* RBA model which additionally considers RNA degradation.

Throughout our study, we consider a fixed molar ribosome mass ω_{R}, but variable rRNA and protein content,

$$\omega_{\mathrm{R}} = n_{\mathrm{rRNA}}\, \omega_{\mathrm{NT}} + n_{\mathrm{rP}}\, \omega_{\mathrm{AA}},$$

and we study the influence of ribosome composition on the cell's maximum growth rate, under the constraints specified above. Here, ω_{NT} and ω_{AA} are the molar masses of nucleotides and amino acids, respectively. For convenience, we define the ribosomal protein (mass) fraction

$$x_{\mathrm{rP}} = n_{\mathrm{rP}} \frac{\omega_{\mathrm{AA}}}{\omega_{\mathrm{R}}}, \tag{4}$$

Table 2. Model parameters for *E. coli* in different media, and for *Thermococcus*. If data for *Thermococcus* was not available, we used *E. coli* parameters from glucose minimal medium. LB, Luria-Bertani medium; Glc+AA, glucose + amino acids medium; Gly+AA, glycerol + amino acids medium; Glc, glucose minimal medium; Gly, glycerol minimal medium; Suc, succinate minimal medium.

Symbol	Name	LB	Glc+AA	Gly+AA	Glc	Gly	Suc	*Thermococcus*	Unit	Source
n_{AA}	ω_{AA}/ω_C	0.61	0.61	1.18	0.61	1.18	0.92	0.61	1	
n_{NT}	$(\omega_{NT}-\omega_{AA})/\omega_C$	1.2	1.2	2.34	1.2	2.34	1.82	1.2	1	
n_{IC}		646						646	1	MC† CPLX-157
n_{EAA}, n_{ENT}		4875						4875	1	Estimate‡
n_{RNAP}		3498						3338	1	***Sutherland and Murakami* (*2018*); *Jun et al.* (*2020*)**
n_{AF}		3900						3900	1	Estimate‡
n_{RNase}		813						813	1	MC† EG11259
ω_C	Molar mass carbon source	180	180	92	180	92	118	180	$g\,mol^{-1}$	
ω_{AA}	Molar mass amino acid	109						109	$g\,mol^{-1}$	BNID§ 104877
ω_{NT}	Molar mass nucleotide	324.3						324.3	$g\,mol^{-1}$	BNID§ 104886
ω_R	Molar mass ribosome	2300000						3040000	$g\,mol^{-1}$	***Kostinski and Reuveni* (*2020*); *Acca et al.* (*1993*)**
k_{IC}^{cat}	Carbon source import rate	180						180	s^{-1}	BNID§ 114686
k_{EAA}^{cat}	Enzyme turnover number	10.5	8.5	7	5	3.5	2	5	s^{-1}	Estimate*
k_{ENT}^{cat}	Enzyme turnover number	10						10	s^{-1}	***Bar-Even et al.* (*2011*)**
k_{RNAP}^{el}	Transcription elongation rate	85						25	$NT\,s^{-1}$	***Bremer and Dennis* (*1996*); *Gehring and Santangelo* (*2017*)**
k_R^{el}	Translation elongation rate	21						8.3	$AA\,s^{-1}$	***Bremer and Dennis* (*1996*), ******
k_{AF}^{cat}	Ribosome assembly rate	1/120						1/120	s^{-1}	BNID§ 102321
k_{RNase}^{deg}	RNase degradation rate	88						88	$NT\,s^{-1}$	***Fazal et al.* (*2015*)**
f_{RNAP}^{act}	RNAP activity	0.31	0.242	0.188	0.15	0.144	0.132	0.15	1	***Kostinski and Reuveni* (*2020*)**
f_R^{act}	Ribosome activity	0.85						0.85	1	***Kostinski and Reuveni* (*2020*)**
$\bar{k}_{RNAP}^{el}$	Effective transcription elongation rate $\bar{k}_{RNAP}^{el} = f_{RNAP}^{act} k_{RNAP}^{el}$	26.35	20.57	15.98	12.75	12.24	11.22	12.75	$NT\,s^{-1}$	
$\bar{k}_R^{el}$	Effective translation elongation rate $\bar{k}_R^{el} = f_R^{act} k_R^{el}$	17.85						17.85	$AA\,s^{-1}$	
K	Half-saturation constant	0.2						0.2	1	

† MetaCyc ID (***Caspi et al., 2018***).

‡ estimated from an average protein length of 325 amino acids (BNID 108986) and an approximate number of proteins involved in amino acid/nucleotide synthesis (https://www.genome.jp/kegg/), or ribosome assembly (***Choi et al., 2020***).

§ BioNumbers ID (***Milo et al., 2009***).

* To consider the nutrient qualities of the differnt media, we assumed that k_{EAA}^{cat} is proportional to the experimental growth rates (Suc: 0.4, Gly: 0.7, Glc:1, Gly+AA:1.4, Glc+AA: 1.7, LB: 2.1 h^{-1}). The growth rates were multiplied by 5 so that the maximum k_{EAA}^{cat} corresponds to the average enzyme turnover rate of 10 (***Bar-Even et al., 2011***).

** An experimentally measured translation rate for *Thermococcus* is unavailable. However, archaeal transcription and translation are likely coordinated, similar to bacteria (***French et al., 2007***; ***Proshkin et al., 2010***). This suggests an upper bound for the translation rate at approximately $25/3 \approx 8.3\,AA\,s^{-1}$.

and express n_{rRNA} and n_{rP} by x_{rP},

$$n_{rRNA} = (1 - x_{rP})\,\frac{\omega_R}{\omega_{NT}} \quad \text{and} \quad n_{rP} = x_{rP}\,\frac{\omega_R}{\omega_{AA}}.$$

In our analysis, we vary ribosomal protein fraction and maximize growth rate under given constraints. Modeling details can be found in section Methods/subsection Model details, the stoichiometric, capacity, and (dry) mass constraints are summarized in ***Table 1***, and the parameter values are given in ***Table 2***.

Base model recovers linear correlation of RNA to protein ratio with growth rate

With parameters for *E. coli* in different media (listed in ***Table 2***) and the experimentally observed ribosome composition ($x_{rP} = 0.36\,\%$), the base model correctly recovers the well-known linear dependence of the RNA to protein ratio and growth rate (***Scott et al., 2010***), see ***Figure 2a***, but not the offset at zero growth rate, since our model does not contain any non-growth associated processes.

To further test the model, we predict RNAP fluxes (v_{RNAP}) at various non-optimal growth rates in glucose minimal medium. In particular, we compute alternative solutions to the system of (in)equalities (1) and (2). (Technically, these solutions are elementary growth vectors (EGVs) as defined in ***Müller et al.* (*2022*)**.) We observe three lines (***Figure 2b***). Two lines (in gray) correspond to solutions where either ribosomes or rRNA accumulate (in excess of what is needed) to support growth. In other words, constraints (2d) and (2b) (rows "cap R" and "rRNA" in ***Table 1***) are not limiting. With increasing growth rate, the excess of rRNA and ribosome decreases, reaching zero at

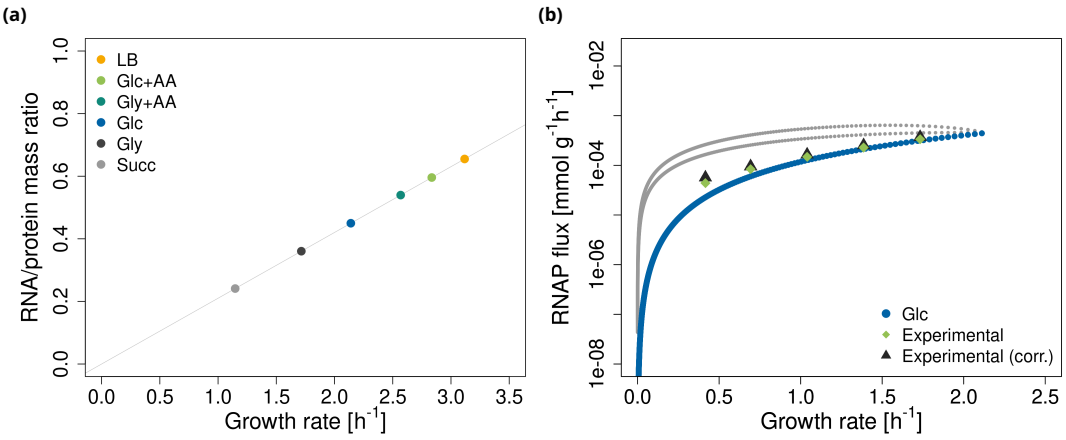

Figure 2. Validation of the base model. **(a)** The model predicts a linear relationship between RNA to protein ratio and growth rate. The points represent maximum growth rates in six experimental conditions (***Table 2***). **(b)** Alternative RNAP fluxes at different non-optimal growth rates in glucose minimal medium. Grey and blue lines are simulations. The blue line corresponds to solutions, where rRNA and ribosomes do not accumulate (constraints "rRNA" and "cap R" in ***Table 1*** are limiting). Light green diamonds are experimental data from ***Bremer and Dennis*** (***1996***), black triangles are data from ***Bremer and Dennis*** (***1996***) corrected for rRNA degradation (***Gausing, 1977***). Data converted to $\mathrm{mmol\,g^{-1}\,h^{-1}}$ with *E. coli* dry masses from ***Milo and Phillips*** (***2015***).

the maximum growth rate. The third line (in blue) corresponds to no accumulation of ribosomes or rRNA. In particular, the RNAP flux exactly matches the demand. At maximum growth rate, all lines converge to one optimal value.

For higher growth rates, experimental data are best fit by the line without accumulation of ribosomes or rRNA. In fact, the accumulation of free rRNA in a cell is biologically not realistic as it is immediately bound by rP during transcription (***Bremer and Dennis, 1996***). While cells do contain approximately 15-20% inactive ribosomes, this fraction remains constant regardless of the growth rate (***Bremer and Dennis, 1996***; ***Kostinski and Reuveni, 2020***). In our model, we have already incorporated this fraction using effective translation elongation rates, see (see ***Table 1***). Therefore, the disagreement between experimental and simulated data at lower growth rates is probably caused by neglecting other types of RNA. Indeed, RNAP allocation to the synthesis of different types of RNA changes with growth rate (***Kostinski and Reuveni, 2020***).

Base model predicts maximal growth for RNA-only ribosomes

We study the dependence of maximum growth rate on the ribosomal protein fraction using the base model described above. We find that, for realistic parameters from *E. coli* (***Table 2***), rRNA synthesis is cheaper than protein synthesis for all tested growth conditions (see ***Figure 3a***). Thus, according to our base model, ribosomes should consist of rRNA only. Indeed, it has been suggested that higher growth rates could be achieved if ribosomes were to consist only of rRNA (***Reuveni et al., 2017***).

If we (hypothetically) adjust the parameters to make rRNA synthesis more expensive than protein synthesis (e.g. by decreasing $\bar{k}^{\mathrm{el}}_{\mathrm{RNAP}}$ or increasing $\bar{k}^{\mathrm{el}}_{\mathrm{R}}$), then maximum growth rate is achieved for a protein-only ribosome (Appendix 1, ***Figure 1***). By a symbolic analysis, we can rigorously prove that maximum growth rate is generically attained at an "exclusive" ribosome composition, either at $x_{\mathrm{rP}} = 0\%$ or $x_{\mathrm{rP}} = 100\%$, regardless of the parameters (see section Methods/subsection Symbolic analysis of growth rate maximization).

To conclude, RBA with standard capacity constraints does not explain mixed (RNA + protein) ribosomes. Thus, additional constraints are needed.

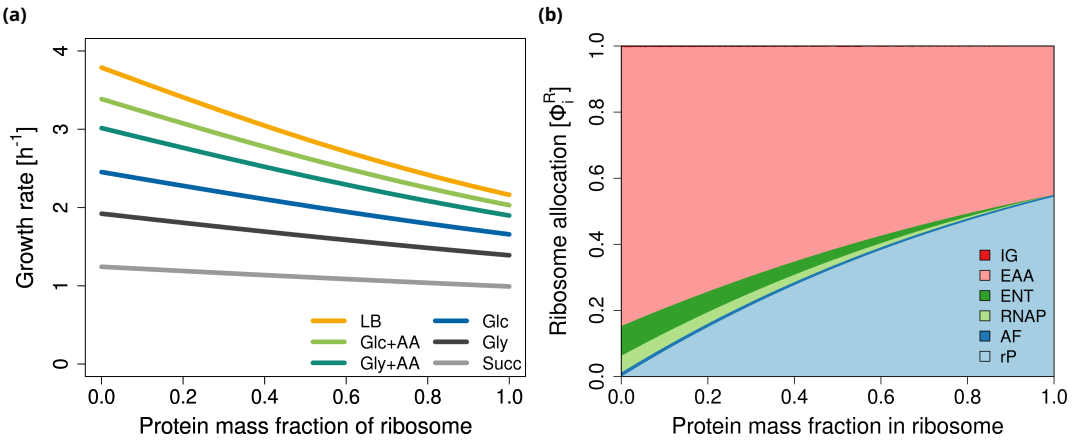

Figure 3. Base model. Maximum growth rate and ribosome allocations as functions of ribosomal protein fraction x_{rP}. **(a)** Maximum growth rate for *E. coli* in six different conditions (see ***Table 2***). **(b)** Ribosome allocations ϕ_i^{R} as defined in Eqn. (3), for glucose minimal medium (Glc).

rRNA instability leads to maximal growth for mixed ribosomes

As one potential explanation, we hypothesize that the different stabilities of rPs and rRNA affect the composition of the ribosome. While proteins are known to be highly stable (***Milo and Phillips, 2015***), rRNA is susceptible to degradation by RNases, which are ubiquitous in cells (***Jain, 2018***). Even at maximum growth, about $10\,\%$ of rRNA is still degraded, and, thus, cannot be incorporated into the ribosome (***Gausing, 1977***; ***Jain, 2018***). Furthermore, rRNA can easily misfold, rendering it inactive and prone to degradation (***Shajani et al., 2011***; ***Rodgers and Woodson, 2021***).

To account for rRNA degradation, we introduce an RNase enzyme that breaks down rRNA into individual nucleotides (NT), via the reaction

$$r_{\mathrm{RNase}}:\ \mathrm{rRNA} \overset{\mathrm{RNase}}{\rightarrow} n_{\mathrm{rRNA}} \cdot \mathrm{NT},$$

see ***Figure 1a***. Since RNases are essential for quality control, we assume some minimum activity and add a minimum degradation rate,

$$v_{\mathrm{RNase}} \geq k^{\mathrm{deg}}(1 - x_{\mathrm{rP}})\, c_{\mathrm{R}}, \tag{5}$$

to the list of constraints (row "min deg" in ***Table 1***). In the simplest case, this rate is directly proportional (with a constant k^{deg}) to the rRNA concentration. The latter is given by the fraction of rRNA in the ribosome concentration, since there is no free rRNA in the cell (***Bremer and Dennis, 1996***). Additionally, $k^{\mathrm{deg}} = k^{\mathrm{deg}}(x_{\mathrm{rP}})$ can be a (monotonically decreasing) function of x_{rP},

$$k^{\mathrm{deg}}(x_{\mathrm{rP}}) = k^{\mathrm{deg}}_{\mathrm{max}} \left(1 - \frac{x_{\mathrm{rP}}^n}{K^n + x_{\mathrm{rP}}^n}\right) \tag{6}$$

modeling the cooperative protection of rRNA by proteins. As for the other enzymes, we add a capacity constraint for the RNase to account for its cost,

$$n_{\mathrm{rRNA}}\, v_{\mathrm{RNase}} \leq k^{\mathrm{deg}}_{\mathrm{RNase}}\, c_{\mathrm{RNase}}, \tag{7}$$

where we use $k^{\mathrm{deg}}_{\mathrm{RNase}} = 88\,\mathrm{NT\,s^{-1}}$ of an enzyme called RNase R (***Fazal et al., 2015***). The *base* RBA model together with RNA degradation, RNase synthesis, and constraints (5) and (7) constitutes the *extended* RBA model.

Taking rRNA degradation into account leads to maximum growth rates at mixed (RNA+protein) ribosome compositions (***Figure 4***). As it turns out, the assumption of a constant k^{deg} in constraint (5) leads to a very shallow optimum (***Figure 4a***). To account for the stabilizing influence of rPs on

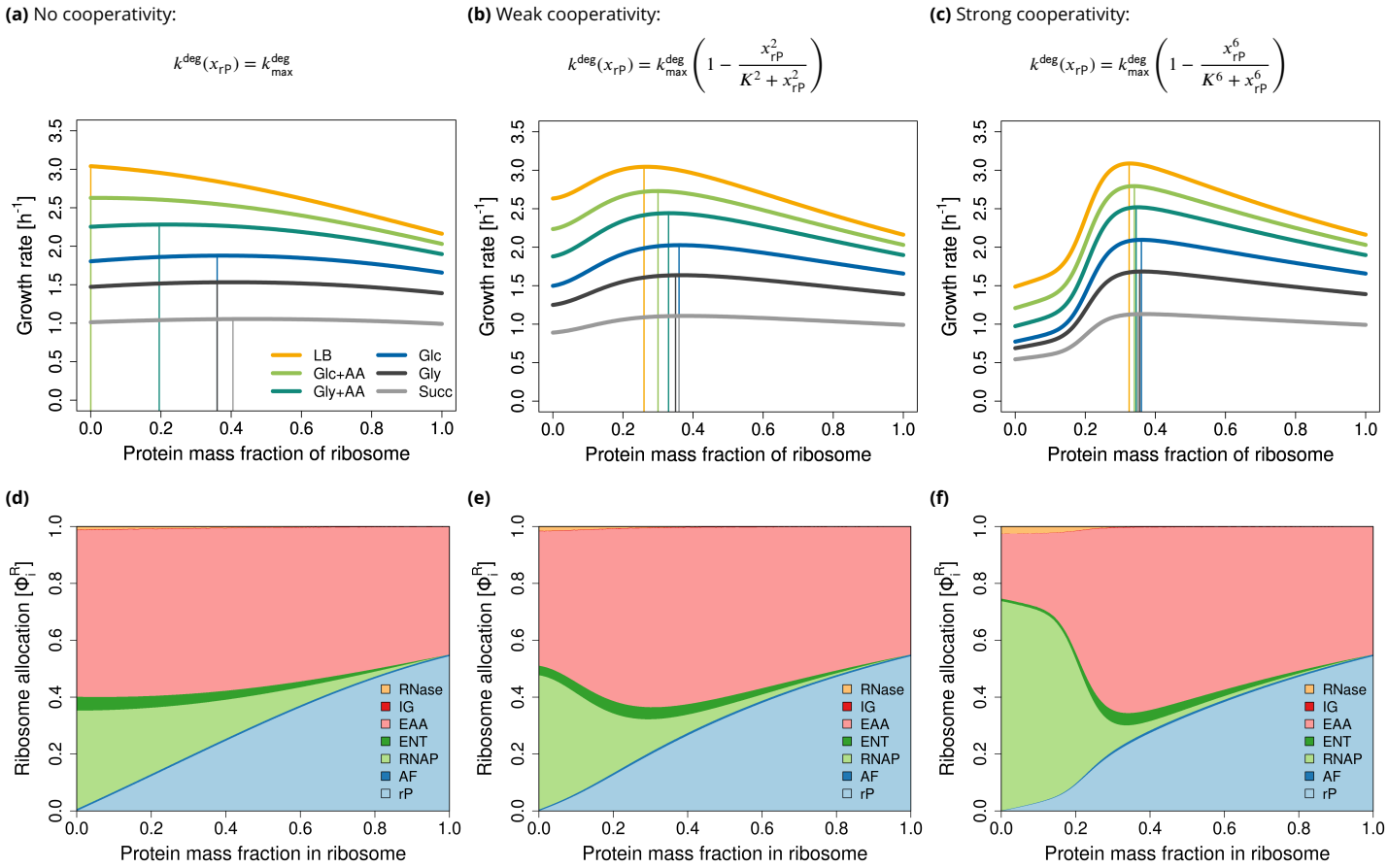

Figure 4. Extended model. Accounting for RNA degradation leads to a mixed (RNA+protein) ribosome composition. **(a-c)** Maximum growth rate of *E. coli* in six different conditions (see ***Table 2***). **(d-f)** Ribosome allocations in glucose minimal medium (Glc). At low protein fractions, rRNA degradation is high, and RNAP (light green) takes up a significant amount of cellular resources.

the folded structure, we introduce the non-linear (Hill-type) degradation term (Equation (6) with half-saturation $K = 0.2$ and Hill-factors $n = 2$ or $n = 6$), leading to a pronounced optimum, see ***Figure 4b*** and ***Figure 4c***.

In the following, we investigate how the optimal ribosome composition depends on growth conditions.

First, we study growth on glucose minimal medium and adjust k^{deg}_{max} such that the optimal ribosome composition matches the experimentally observed value of $x_{rP} = 0.36$ for *E. coli*. We validate the model for the three types of degradation, and we correctly predict the linear dependence of the RNA to protein ratio on growth rate (Appendix 1, ***Figure 2***). However, RNAP flux predictions are only realistic when assuming strong cooperativity ($n = 6$). For the other two cases, rRNA degradation in the optimum is too high which leads to overestimated RNAP fluxes (Appendix 1, ***Figure 3***).

Second, we predict maximum growth rate as a function of the ribosomal protein fraction in five different growth media. We find that the more proteins cooperate, the less the optimal ribosome composition depends on the growth conditions, see ***Figure 4***(a-c).

Third, to further understand these results, we plot ribosome allocations for glucose minimal medium, see ***Figure 4***(d-f). Interestingly, at low x_{rP}, a significant fraction of ribosomes is allocated to the production of RNAP, whereas with increasing x_{rP}, this ribosome allocation rapidly drops. In the case of the highest cooperativity, allocations at the optimal x_{rP} are comparable to the base RBA model (without RNA degradation), compare ***Figure 4f*** with ***Figure 3b***.

Finally, we qualitatively predict that the fraction of degraded rRNA decreases with growth rate

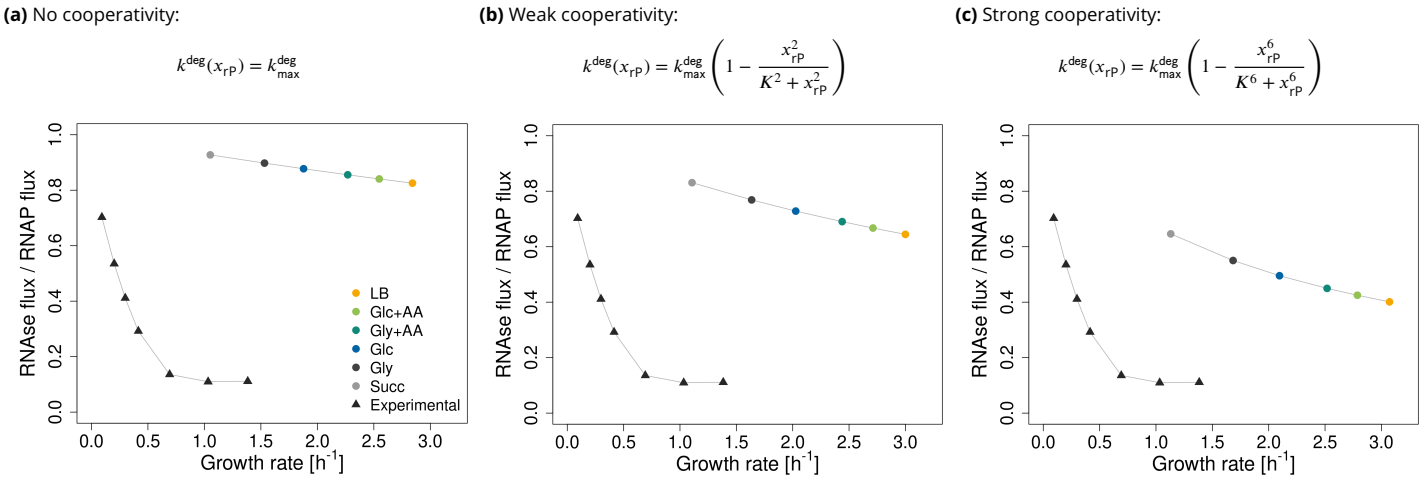

Figure 5. The extended model recapitulates the experimentally observed decrease in the fraction of degraded RNA with increasing growth rate. The circles are the predicted ratios of RNAse fluxes to RNAP fluxes at different conditions. The triangles represent experimental data from ***Gausing*** (***1977***), extracted from the original plot with WebPlotDigitizer (***Rohatgi, 2022***).

(***Figure 5***), which is in agreement with experimental observations (***Gausing, 1977***). This effect gets stronger (and closer to experimental data) with higher rP cooperativity. The quantitative disagreement between the experimental and predicted values is probably due to the simplicity of our model. For example, it does not include other types of RNA or regulatory processes, both of which influence RNAP activity. If we consider RNAP allocation to rRNA ($\bar{k}^{el}_{RNAP} = k^{el}_{RNAP} f^{act}_{RNAP} \phi^{RNAP}_{rRNA}$), the results get closer to experimental data (Appendix 1, ***Figure 4***).

Based on these results, we conclude that accounting for RNA degradation and cooperative binding of rP can explain the mixed ribosome composition.

Extreme conditions increase the optimal protein fraction in (archaeal) ribosomes

As a straightforward extension, we explore whether the current model can be adapted to predict the ribosome composition of other organisms. For example, archaeal ribosomes contain $36\,\%$–$50\,\%$ protein (***Acca et al., 1993***), eukaryotic ribosomes $42\,\%$–$50\,\%$ protein (***Wilson and Cate, 2012***; ***Verschoor et al., 1998***; ***Reuveni et al., 2017***), and mitochondrial ribosomes $51\,\%$–$89\,\%$ protein. We ask whether this variability can be explained by efficient resource allocation.

It has been hypothesized that the extra archaeal/eukaryotic ribosomal proteins primarily serve to stabilize the ribosomes (***Kisly and Tamm, 2023***). This may be particularly important for archaea because they commonly live in extreme conditions, such as high temperatures or low pH, which may lead to higher (misfolding and) degradation of RNA. To mitigate this, archaea might need a higher protein content compared to bacteria. It has been shown that the initial steps in ribosome assembly of the thermophilic archaeon *Sufolobus solfataricus* do not require high temperature and likely involve core proteins that are also present in bacteria. However, completing the assembly requires high temperature, suggesting that these proteins have evolved to cope with such extreme conditions (***Altamura et al., 1991***; ***Londei et al., 1986***).

We model this process by increasing k^{deg}_{max} which leads to a higher predicted protein content of the ribosome (***Figure 6***). Similarly to *E. coli*, the higher the cooperativity, the lower the sensitivity of the optimum to the other parameters. Moreover, when using parameters from *Thermococcus* (see ***Table 2***), we observe an increase in ribosomal protein content, in accordance with experimental evidence (***Acca et al., 1993***), and predict a decrease in growth rate.

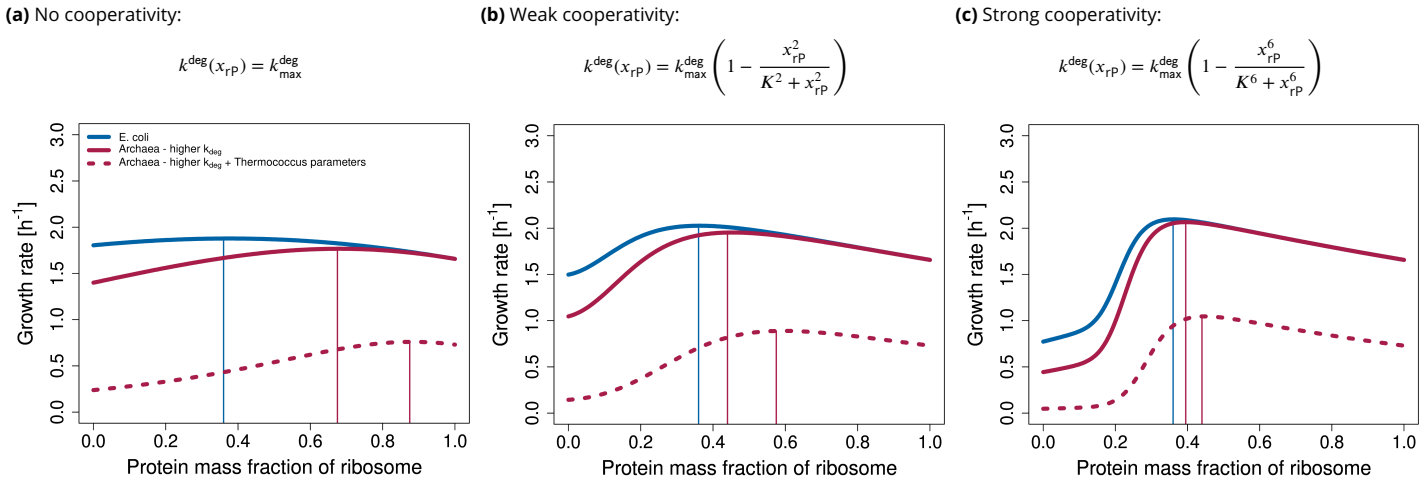

Figure 6. The model can be adjusted to predict archaeal protein-rich ribosome composition. The model was adapted to archaea by increasing k^{deg}_{max} two-fold. The remaining parameters were either kept the same as in *E. coli* (red solid line), or parameters from *Thermococcus* (molecular masses of R and RNAP, transcription and translation rates, see ***Table 2***) were used (red dashed line).

Discussion

The ribosome is a central player in cellular self-fabrication, placing an upper bound on growth rate. To grow faster, a cell needs more ribosomes which, in turn, requires even more ribosomes to produce themselves. While most catalysts and molecular machines within a cell are proteins, ribosomes stand out by having a significant (mass) fraction of rRNA, playing a catalytic role. The mass fraction of rPs varies across kingdoms, ranging from approximately $36\,\%$ in prokaryotes (***Kurland, 1960***) to around $50\,\%$ in eukaryotes (***Wilson and Cate, 2012***), and even higher in eukaryotic mitochondria, reaching up to $89\,\%$ in *Trypanosoma brucei* (***Moore, 2019***; ***Ramrath et al., 2018***). This prompts the question: what factors determine the ratio of RNA to protein in ribosomes?

The analysis of our base model (without RNA degradation) suggests that RNA-only ribosomes maximize growth rate (***Figure 3a***). This results from the lower cost of rRNA synthesis compared to rP synthesis. It remains true even when one accounts for the synthesis of inactive RNAP and enzymes required for nucleotide synthesis (***Reuveni et al., 2017***), which suggests that the costs of rRNA synthesis and associated processes are underestimated in the base model.

In order to explain a mixed (RNA+protein) ribosome, we consider rRNA degradation in our extended model, thereby increasing the costs for RNA synthesis. Indeed, it has been experimentally observed that even at maximum growth rate, $10\,\%$ of newly synthesized rRNA is degraded (***Gausing, 1977***). Due to the extremely high rates at which rRNA is synthesized, errors become inevitable, necessitating the action of quality control enzymes such as polynucleotide phosphorylase (PNPase) and RNase R to ensure ribosome integrity (***Dos Santos et al., 2018***). The absence of the RNases results in the accumulation of rRNA fragments, ultimately leading to cell death (***Cheng and Deutscher, 2003***; ***Jain, 2018***). In our resource balance approach, decreasing the RNA content of the ribosome saves resources by reducing RNA turnover. At the same time, protein synthesis costs increase, leading to a mixed (RNA+protein) ribosome at maximum growth rate.

We include RNA degradation in two scenarios. (a) RNA is degraded at a rate proportional to its concentration, or (b) RNA degradation rate decreases non-linearly with ribosomal protein content, since proteins cooperatively protect RNA from degradation (***Shajani et al., 2011***; ***Bowman et al., 2015***; ***Rodgers and Woodson, 2019***). Both versions of the model predict an optimal mixed (RNA+protein) ribosome. However, without considering cooperative protein binding, optimal ribosome compositions depend on growth conditions. Notably, the higher the cooperativity, the closer the predicted RNAP fluxes and the fraction of degraded rRNA are to experimental data. Yet,

more experimental data is needed to decide whether ribosome composition in *E. coli* remains truly independent of growth conditions when the bacterium is evolutionarily adapted to a single environment. Based on these results and available experimental evidence for cooperative protein binding (***Rodgers and Woodson, 2019***), we conclude that scenario (b) is more likely.

Our simple model lumps ribosome assembly and RNA degardation and hence allows multiple explanations for the precise mechanism. On the one hand, proteins may stabilize RNA either by blocking the access of RNases to RNA or by preventing misfolding. Intuitively, this could be explained by the fact that RNA molecules are long, and in order to protect them from misfolding and degradation, a certain critical amount of proteins is needed. Folding intermediates can get trapped in misfolded states and are subsequently degraded as a part of quality control. Proteins may help RNA to avoid these kinetic traps (***Bushhouse et al., 2022***; ***Abeysirigunawardena et al., 2017***; ***Shajani et al., 2011***; ***Rodgers and Woodson, 2021***). On the other hand, proteins may increase the rate of ribosome assembly and thereby reduce the number of ribosome intermediates (pre-R in ***Figure 7***). Indeed, it was observed that rRNA can fold to near-native conformation (***K. Lenz et al., 2017***; ***Adilakshmi et al., 2005***). Yet, this process is slower than the protein-supported one, especially for long molecules (***Hyeon and Thirumalai, 2012***; ***Rodgers and Woodson, 2021***).

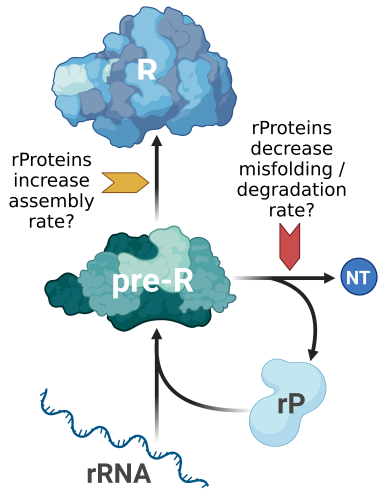

Figure 7. Potential mechanisms by which ribosomal proteins affect the biosynthesis of ribosomes.

Throughout the manuscript, we make use of two simplifications:

- As in ***Kostinski and Reuveni*** (***2020***), we consider ribosomes with different compositions, but equal mass. RNA enzymes, known as ribozymes, are generally smaller than proteins and require only a few nucleotides for catalytic activity (***Bernhardt, 2012***). However, such small ribozymes are also inefficient. Increasing their size often improves turnover number, but may impede folding (***Martick and Scott, 2006***; ***Hyeon and Thirumalai, 2012***; ***Jeffares et al., 1998***). Therefore, we consider the case of a large, hard-to-fold, but catalytically efficient RNA-only ribosome.
- We do not consider the effect of protein content on catalytic rates of the ribosomes. Proteins are generally more efficient catalysts than ribozymes (***Jeffares et al., 1998***), yet rRNA is still present in the peptidyl transferase center (***Tirumalai et al., 2021***), and translation rate does not increase in ribosomes with a higher protein content (***Bonven and Gulløv, 1979***; ***Hartl and Hayer-Hartl, 2009***). Furthermore, despite the modest catalytic rate of peptide bond formation, it does not appear to be the rate-limiting step. Given the size of the substrate molecules (mRNA), diffusion may be the limiting factor (***Bernhardt and Tate, 2015***; ***Jeffares et al., 1998***). Therefore, we assume that enhancing ribosome catalytic rate is not the main reason for the addition of proteins. However, it is possible that proteins stabilize the ribosome structure

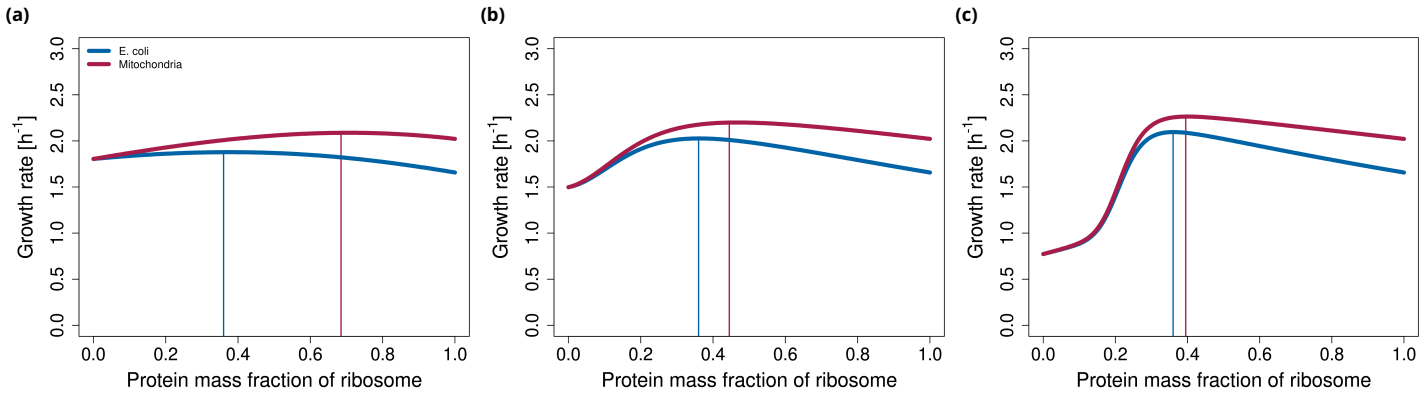

Figure 8. The model can be adjusted to predict mitochondrial protein-rich ribosome composition. For simplicity, we assumed that 1/3 of rP are imported for free from cytoplasm. (In reality, almost all rP are imported, but mitochondria make additional proteins to provide energy for the whole cell.)

and thereby indirectly ensure efficient peptide bond formation (***Jeffares et al., 1998***).

In future versions of the model, these assumptions can be relaxed. Furthermore, incorporating other types of RNA (mRNA, tRNA) and energy metabolism, or even constructing a genome-scale RBA model (***Hu et al., 2020***), will likely lead to more quantitative predictions of fluxes and growth rate.

To better model protein-rich organisms such as archaea, the model could be expanded by including the temperature dependence of rRNA degradation and assembly in more detail. Apart from $k_{\text{max}}^{\text{deg}}$, other parameters (e.g. K or n in the Hill function) might change too to capture the effects of extreme conditions. Furthermore, the effects of other extreme conditions (such as pH and osmolarity), and the reasons for the variability of archaeal ribosome composition could also be investigated (***Greber et al., 2012***; ***Londei and Ferreira-Cerca, 2021***). However, the predictions of our current model are in agreement with the naive expectation that more proteins are required to keep ribosomes stable in harsh conditions. More experimental data is needed to model the archaeal ribosomes realistically.

In mitochondria, a higher protein content may be advantageous since rP are not made directly in mitochondria, but are imported "for free" from the cytoplasm (***Woellhaf et al., 2014***). In other words, mitochondria can afford to have additional proteins without impacting growth rate and thereby gain additional functionality (e.g. regulation). Indeed, when we allow a "free" import of rP in our model, we observe that the optimum moves towards a protein-rich ribosome (***Figure 8***). However, in order to accurately model mitochondria, it is essential to model the synthesis of cytoplasmic (eukaryotic) ribosomes, several types of RNA polymerases, and the dynamic interaction between host cells and mitochondria. While the cytoplasm provides ribosomal proteins for mitochondria, mitochondria synthesize enzymes of oxidative phosphorylation and provide ATP back to the host cell. Furthermore, it will be necessary to consider other roles of proteins, such as regulation, signaling, and other specialized functions of the ribosomal proteins.

Formal comparison with *Kostinski and Reuveni* (*2020*)

Our analysis is motivated by the previous work of ***Kostinski and Reuveni*** (***2020***), who understand ribosome composition as a competition between two autocatalytic loops. One loop is responsible for synthesizing rRNA, while the other loop is responsible for rP synthesis, both competing for limited resources. These loops and their constraints, namely, the stoichiometric constraints for rRNA and rP and the capacity constraint for RNAP, are contained in our more detailed RBA model, see ***Table 1***. In addition to these three conditions, ***Kostinski and Reuveni*** (***2020***) make two more

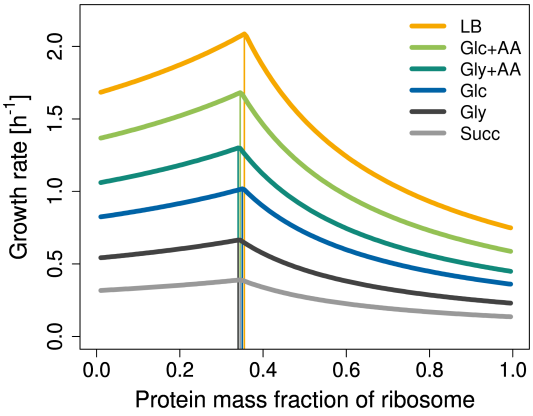

Figure 9. The base RBA model with fixed ribosome allocations and parameters from ***Kostinski and Reuveni*** (***2020***) in multiple growth conditions. For the definition of the ribosome allocations $\phi^{\mathrm{R}}_{\mathrm{rP}}$ and $\phi^{\mathrm{R}}_{\mathrm{RNAP}}$ see Eqn. (3). For the parameter values $(k^{\mathrm{el}}_{\mathrm{R}}, f^{\mathrm{act}}_{\mathrm{R}}, \phi^{\mathrm{R}}_{\mathrm{rP}})$ and $(k^{\mathrm{el}}_{\mathrm{RNAP}}, f^{\mathrm{act}}_{\mathrm{RNAP}}, \phi^{\mathrm{R}}_{\mathrm{RNAP}}, \phi^{\mathrm{RNAP}}_{\mathrm{rRNA}})$, see the original paper.

assumptions: they fix the "ribosome allocations" $\phi^{\mathrm{R}}_{\mathrm{rP}}$ and $\phi^{\mathrm{R}}_{\mathrm{RNAP}}$ for the synthesis of rP and RNAP, defined in Eqn. (3).

The resulting upper limits on growth rate can be derived easily by considering the synthesis of rRNA and rP, separately.

(rP) The stoichiometric constraint for rP is given by $\upsilon_{\mathrm{AF}} \leq w_{\mathrm{rP}}$, see ***Table 1***. Together with the definition of the corresponding ribosome allocation $\phi^{\mathrm{R}}_{\mathrm{rP}} = \frac{\mu\, n_{\mathrm{rP}}\, w_{\mathrm{rP}}}{\bar{k}^{\mathrm{el}}_{\mathrm{R}}\, \upsilon_{\mathrm{AF}}}$, this yields

$$\mu \leq \frac{\bar{k}^{\mathrm{el}}_{\mathrm{R}}\, \phi^{\mathrm{R}}_{\mathrm{rP}}}{n_{\mathrm{rP}}}. \tag{8a}$$

(rRNA) The stoichiometric constraint for rRNA and the capacity constraint for RNAP are given by $\upsilon_{\mathrm{AF}} \leq \upsilon_{\mathrm{RNAP}}$ and $\mu\, n_{\mathrm{rRNA}}\, \upsilon_{\mathrm{RNAP}} \leq \bar{k}^{\mathrm{el}}_{\mathrm{RNAP}}\, w_{\mathrm{RNAP}}$, see ***Table 1***. By multiplication, they imply $\mu\, n_{\mathrm{rRNA}}\, \upsilon_{\mathrm{AF}} \leq \bar{k}^{\mathrm{el}}_{\mathrm{RNAP}}\, w_{\mathrm{RNAP}}$. Together with the definition of the ribosome allocation $\phi^{\mathrm{R}}_{\mathrm{RNAP}} = \frac{\mu\, n_{\mathrm{RNAP}}\, w_{\mathrm{RNAP}}}{\bar{k}^{\mathrm{el}}_{\mathrm{R}}\, \upsilon_{\mathrm{AF}}}$ for the synthesis of RNAP, this yields

$$\mu^2 \leq \frac{\bar{k}^{\mathrm{el}}_{\mathrm{R}}\, \bar{k}^{\mathrm{el}}_{\mathrm{RNAP}}\, \phi^{\mathrm{R}}_{\mathrm{RNAP}}}{n_{\mathrm{rRNA}}\, n_{\mathrm{RNAP}}}. \tag{8b}$$

These upper bounds (8) are Eqns. (2) and (5) in ***Kostinski and Reuveni*** (***2020***), after inserting the effective transcription and translation elongation rate constants $\bar{k}^{\mathrm{el}}_{\mathrm{RNAP}} = k^{\mathrm{el}}_{\mathrm{RNAP}}\, f^{\mathrm{act}}_{\mathrm{RNAP}}\, \phi^{\mathrm{RNAP}}_{\mathrm{rRNA}}$ and $\bar{k}^{\mathrm{el}}_{\mathrm{R}} = k^{\mathrm{el}}_{\mathrm{R}}\, f^{\mathrm{act}}_{\mathrm{R}}$, respectively. Here, $\phi^{\mathrm{RNAP}}_{\mathrm{rRNA}}$ denotes the fraction of RNAP transcribing rRNA (which we assume to equal one in the rest of this work).

Using Eqn. (4), the two upper bounds (8) can be written as functions of the rP fraction x_{rP}, namely as

$$\mu \leq \gamma_{\mathrm{rP}} \frac{\phi^{\mathrm{R}}_{\mathrm{rP}}}{x_{\mathrm{rP}}} \quad \text{and} \quad \mu \leq \gamma_{\mathrm{RNAP}} \sqrt{\frac{\phi^{\mathrm{R}}_{\mathrm{RNAP}}}{1 - x_{\mathrm{rP}}}} \tag{9}$$

with constants $\gamma_{\mathrm{rP}}, \gamma_{\mathrm{RNAP}} > 0$. For fixed "ribosome allocations" $\phi^{\mathrm{R}}_{\mathrm{rP}}$ and $\phi^{\mathrm{R}}_{\mathrm{RNAP}}$, the two curves necessarily intersect at some $0 < x^{*}_{\mathrm{rP}} < 1$, and $\mu(x^{*}_{\mathrm{rP}})$ is the maximum growth rate allowed by the constraints considered above, namely the stoichiometric constraints for rP and rRNA and the RNAP capacity constraint.

Kostinski and Reuveni (***2020***) interpret Eqns. (9) as a trade-off between rRNA and rP production. This effect arises because they fix the ribosome allocations. In particular, ***Kostinski and Reuveni*** (***2020***) fix $\phi^{\mathrm{R}}_{\mathrm{rP}}$ and $\phi^{\mathrm{R}}_{\mathrm{RNAP}}$ to experimental values for *E. coli* (in multiple growth conditions), and find that maximum growth rate occurs close to the current rP fraction ($x_{\mathrm{rP}} = 36\%$), and the resulting $\mu(x_{\mathrm{rP}})$ is close to the experimental value. If we use their parameters (see ***Table 2***), we can exactly reproduce their results (see ***Figure 9***). Our base model provides an explanation for the protein investment costs, giving a proper mechanistic interpretation to the argument presented by ***Kostinski***

and Reuveni (***2020***). Moreover, it is closer to an evolutionary scenario, where a cell can adjust both ribosome composition x_{rP} and ribosome allocations ϕ^{R}. However, the base model predicts an optimal ribosome that is RNA-only (for realistic parameters), see ***Figure 3a***. This is possible because the ribosome allocations are adjusted according to demand. The ribosome allocations corresponding to varying ribosomal protein fraction are illustrated in ***Figure 3b***. Only the extended model with RNA degradation predicts a mixed (RNA+protein) ribosome at maximum growth rate.

Methods

Our analysis is based on the small model of a self-replicating cell depicted in ***Figure 1*** and described below. Constraints are listed in ***Table 1*** and parameters in ***Table 2***. For an introduction to resource allocation in next-generation models of cellular growth, including the definition of EGVs, see ***Müller et al.*** (***2022***). EGVs were enumerated using the package efmtool 0.2.0 (***Terzer and Stelling, 2008***) in Python 3.8.13. ***Figure 1a*** was created with `BioRender.com` and the remaining figures with R version 4.1.2. All code is available at https://github.com/diana-sz/RiboComp.

Model details

We consider the small model of a self-fabricating cell depicted in ***Figure 1a*** which contains metabolic reactions and macromolecular synthesis reactions. To take into account the limitation of cellular resources, we use three types of capacity constraints: enzyme capacity constraints limit the rate of metabolic reactions, the RNAP capacity constraint limits transcription rate, and the ribosome capacity constraint limits the synthesis rates of all proteins (including the ribosomal proteins).

The cell takes up a carbon source (C) via the reaction

$$r_{\mathrm{IC}}: \quad \overset{\mathrm{IC}}{\rightarrow} \mathrm{C},$$

catalyzed by the importer IC, and forms amino acids (AA), nucleotides (NT), and ribosomal RNA (rRNA) via

$$r_{\mathrm{EAA}}: \quad n_{\mathrm{AA}} \cdot \mathrm{C} \overset{\mathrm{EAA}}{\rightarrow} \mathrm{AA}, \qquad r_{\mathrm{ENT}}: \quad n_{\mathrm{NT}} \cdot \mathrm{C} + \mathrm{AA} \overset{\mathrm{ENT}}{\rightarrow} \mathrm{NT}, \qquad r_{\mathrm{RNAP}}: \quad n_{\mathrm{rRNA}} \cdot \mathrm{NT} \overset{\mathrm{RNAP}}{\rightarrow} \mathrm{rRNA},$$

catalyzed by the enzymes EAA, ENT, and the RNA polymerase (RNAP). Ultimately, the ribosome R is built from rRNA and ribosomal protein (rP) via

$$r_{\mathrm{AF}}: \quad \mathrm{rRNA} + \mathrm{rP} \overset{\mathrm{AF}}{\rightarrow} \mathrm{R},$$

catalyzed by the assembly factors AF. The processes above are part of the "base model". In an "extended model", ribosomal RNA degrades via

$$r_{\mathrm{RNase}}: \quad \mathrm{rRNA} \overset{\mathrm{RNase}}{\rightarrow} n_{\mathrm{rRNA}} \cdot \mathrm{NT},$$

catalyzed by the RNase. Finally, we consider the *synthesis* of all proteins (enzymes and ribosomal protein) via the reactions

$$s_i: \quad n_i \cdot \mathrm{AA} \overset{\mathrm{R}}{\rightarrow} i, \quad i \in \mathrm{Proteins} = \{\mathrm{IC}, \mathrm{EAA}, \mathrm{ENT}, \mathrm{RNAP}, (\mathrm{RNase}), \mathrm{AF}, \mathrm{rP}\},$$

catalyzed by the ribosome.

The resulting stoichiometric matrix and the corresponding flux vector are displayed in ***Figure 1b***, and parameter values are given in ***Table 2***. In fact, the stoichiometric matrix can be partitioned into two submatrices,

$$\boldsymbol{N} = \begin{pmatrix} \boldsymbol{N}_{\mathrm{Met}} \\ \boldsymbol{N}_{\mathrm{Cat}} \end{pmatrix},$$

corresponding to the "metabolites" $\mathrm{Met} = \{\mathrm{C}, \mathrm{AA}, \mathrm{NT}, \mathrm{rRNA}, \mathrm{rP}\}$ and the catalysts $\mathrm{Cat} = \mathrm{Enz} \cup \{\mathrm{R}\}$ including the "enzymes" $\mathrm{Enz} = \{\mathrm{IC}, \mathrm{EAA}, \mathrm{ENT}, \mathrm{RNAP}, (\mathrm{RNase}), \mathrm{AF}\}$ and the ribosome. By abuse of notation, the flux vector can be partitioned into two subvectors,

$$\boldsymbol{v} = \begin{pmatrix} \boldsymbol{v} \\ \boldsymbol{w} \end{pmatrix},$$

Box 1. Comprehensive models of cellular growth

Comprehensive models of cellular growth (as used in RBA) need not be genome-scale, but involve explicit synthesis reactions for all catalysts. This is in contrast to traditional metabolic models (as used in FBA) which involve an approximate biomass "reaction", thereby fixing biomass composition.

At steady state, the dynamic model of cellular growth yields $\boldsymbol{N}\boldsymbol{v} = \mu\,\boldsymbol{c}$ together with the (dry) mass constraint $\boldsymbol{\omega}^T\boldsymbol{c} = 1$. Thereby, μ is growth rate, $\boldsymbol{v}$ is the vector of fluxes, $\boldsymbol{c}$ is the vector of concentrations, and $\boldsymbol{\omega}$ is the vector of molar masses.

In the constraint-based approach, we consider the (in-)equality system for the fluxes

$$\boldsymbol{N}\boldsymbol{v} \geq \boldsymbol{0}, \quad \boldsymbol{v} \geq \boldsymbol{0}, \quad \text{and} \quad \mu = \boldsymbol{\omega}^T\boldsymbol{N}\boldsymbol{v} = \boldsymbol{\omega}^T\boldsymbol{N}^{\text{exc}}\boldsymbol{v}^{\text{exc}}.$$

Thereby, we assume that all reactions have a given direction, and we use the fact that growth rate is determined by the exchange reactions, cf. ***Müller et al.* (2022)**.

Finally, concentrations are determined by fluxes via $\boldsymbol{c} = \boldsymbol{N}\boldsymbol{v}/\mu$. In particular, concentrations of catalysts are used to formulate additional capacity constraints.

---

corresponding to the enzymatic reactions r and the protein synthesis reactions s.

In general, comprehensive models of cellular growth lead to linear (in-)equality systems for the fluxes, and concentrations are determined by fluxes, see ***Box 1***. In the example, we distinguish enzymatic reactions r and protein synthesis reactions s (with corresponding fluxes $\boldsymbol{v}$ and $\boldsymbol{w}$), and further metabolites Met and catalysts Cat, see above. Explicitly, we study the inequality system

$$\begin{pmatrix} \boldsymbol{N}_{\text{Met}} \\ \boldsymbol{N}_{\text{Cat}} \end{pmatrix} \begin{pmatrix} \boldsymbol{v} \\ \boldsymbol{w} \end{pmatrix} \geq \boldsymbol{0}, \quad \boldsymbol{v} \geq \boldsymbol{0},\, \boldsymbol{w} \geq \boldsymbol{0}, \quad \text{and} \quad \mu = \omega_{\text{C}} v_{\text{IC}},$$

since r_{IC} is the only exchange reaction.

In fact, only $\boldsymbol{N}_{\text{Met}}\binom{\boldsymbol{v}}{\boldsymbol{w}} \geq \boldsymbol{0}$ yields non-trivial constraints, since $\boldsymbol{N}_{\text{Cat}}\binom{\boldsymbol{v}}{\boldsymbol{w}} \geq \boldsymbol{0}$ yields $w_i \geq 0$ for $i \in \text{Enz}$ and $v_{\text{AF}} \geq 0$, already included in $\boldsymbol{v} \geq \boldsymbol{0}$, $\boldsymbol{w} \geq \boldsymbol{0}$. However, $\boldsymbol{N}_{\text{Cat}}$ determines the catalyst concentrations via $\mu\,\boldsymbol{c}_{\text{Cat}} = \boldsymbol{N}_{\text{Cat}}\binom{\boldsymbol{v}}{\boldsymbol{w}}$ or, explicitly,

$$c_i = w_i/\mu, \quad i \in \text{Enz}, \qquad \text{and} \qquad c_{\text{R}} = v_{\text{AF}}/\mu. \tag{10}$$

(Recall that the ribosome is formed by the assembly factors.)

Now, catalyst concentrations are used to formulate capacity constraints (for importer, metabolic enzymes, and assembly factors),

$$v_i \leq k_i^{\text{cat}}\, c_i, \quad i \in \{\text{IC}, \text{EAA}, \text{ENT}, \text{AF}\} \subset \text{Enz}, \tag{11a}$$

where k_i^{cat} are the corresponding enzyme turnover numbers. The capacity constraints for the RNA polymerase, (optionally the RNase), and the ribosome are given by

$$n_{\text{rRNA}}\, v_{\text{RNAP}} \leq \bar{k}^{\text{el}}_{\text{RNAP}}\, c_{\text{RNAP}}, \qquad (n_{\text{rRNA}}\, v_{\text{RNase}} \leq k^{\text{deg}}_{\text{RNase}}\, c_{\text{RNase}}), \tag{11b}$$

and

$$\sum_{i \in \text{Proteins}} n_i\, w_i \leq \bar{k}^{\text{el}}_{\text{R}}\, c_{\text{R}}, \tag{11c}$$

respectively. Here, n_{rRNA} is the number of nucleotides in rRNA, and n_i is the number of amino acids in protein i, cf. the stoichiometric coefficients in ***Figure 1b***. Further, $\bar{k}^{\text{el}}_{\text{RNAP}} = k^{\text{el}}_{\text{RNAP}} f^{\text{act}}_{\text{RNAP}}$ and $\bar{k}^{\text{el}}_{\text{R}} = k^{\text{el}}_{\text{R}} f^{\text{act}}_{\text{R}}$ are the effective transcription and translation elongation rate constants, respectively, and $k^{\text{deg}}_{\text{RNase}}$ is the RNA degradation rate constant.

Finally, catalyst concentrations are expressed by corresponding fluxes in all capacity constraints (11) via Eqns. (10). The stoichiometric, capacity, and (dry) mass constraints described so far are summarized in ***Table 1***, and the parameter values are given in ***Table 2***.

In particular, after using (10), the ribosome capacity constraint (11c) takes the form

$$\sum_{i\in\text{Proteins}} \mu\, n_i\, w_i \le \bar{k}_\text{R}^\text{el}\, v_\text{AF},$$

which suggests the definition of "ribosome allocations" (ribosome fractions translating certain proteins),

$$\phi_i^\text{R} = \frac{\mu\, n_i\, w_i}{\bar{k}_\text{R}^\text{el}\, v_\text{AF}}, \quad i \in \text{Proteins}.$$

Obviously, $\sum_{i\in\text{Proteins}} \phi_i^\text{R} \le 1$. Instead of varying the protein synthesis fluxes $\boldsymbol{w}$, one may vary v_AF (the ribosome synthesis flux) and the (vector of) ribosome allocations $\boldsymbol{\phi}^\text{R}$.

Throughout this work, we consider a fixed ribosome mass, but variable ribosomal RNA and protein content,

$$\omega_\text{R} = n_\text{rRNA}\, \omega_\text{NT} + n_\text{rP}\, \omega_\text{AA},$$

where n_rRNA and n_rP are the numbers of nucleotides and amino acids in rRNA and rP, respectively. We define the ribosomal protein (mass) fraction

$$x_\text{rP} = n_\text{rP}\, \frac{\omega_\text{AA}}{\omega_\text{R}},$$

and express n_rRNA and n_rP by x_rP,

$$n_\text{rRNA} = (1 - x_\text{rP})\, \frac{\omega_\text{R}}{\omega_\text{NT}} \quad \text{and} \quad n_\text{rP} = x_\text{rP}\, \frac{\omega_\text{R}}{\omega_\text{AA}}.$$

For variable ribosomal protein fraction x_rP (from 0 to 100%), we maximize growth rate (by varying fluxes under the given constraints).

Symbolic analysis of growth rate maximization

In order to confirm our numerical results, we also perform a symbolic analysis of growth rate maximization.

The "base model" involves five stoichiometric constraints (for the species C, AA, NT, RNAP, rP), six capacity constraints (for the reactions catalyzed by IC, EAA, ENT, RNAP, AF, R), and one (dry) mass constraint, cf. ***Table 1*** (without the columns and rows in red). They define a linear equality and inequality system with 12 constraints (either $\ge$ or $=$) for 11 fluxes and 1 right-hand side.

We apply the determinant method introduced in ***Box 2*** to the resulting matrix $\boldsymbol{B} \in \mathbb{R}^{12\times 12}$, and we find

$$\begin{aligned} 0 = \det \boldsymbol{B} \sim &\left(\left[\frac{n_\text{IC}}{k_\text{IC}^\text{cat}} \frac{\omega_\text{NT}}{\omega_\text{G}} + \frac{n_\text{EAA}}{k_\text{EAA}^\text{cat}} + \frac{n_\text{ENT}}{k_\text{ENT}^\text{cat}} + \frac{n_\text{RNAP}}{\bar{k}_\text{RNAP}^\text{el}} \right] n_\text{rRNA} + \frac{n_\text{AF}}{k_\text{AF}^\text{cat}} \right) \mu^2 \\ &+ \left(\bar{k}_\text{R}^\text{el} \left[\frac{n_\text{IC}}{k_\text{IC}^\text{cat}} \frac{\omega_\text{AA}}{\omega_\text{G}} + \frac{n_\text{EAA}}{k_\text{EAA}^\text{cat}} \right] + n_\text{rP} \right) \mu - \bar{k}_\text{R}^\text{el}. \end{aligned}$$

Using ribosomal protein fraction and rescaling time,

$$n_\text{rRNA} = (1 - x_\text{rP}) \frac{\omega_\text{R}}{\omega_\text{NT}}, \quad n_\text{rP} = x_\text{rP} \frac{\omega_\text{R}}{\omega_\text{AA}}, \quad \text{and} \quad \hat{\mu} = \frac{\mu}{\bar{k}_\text{R}^\text{el}} \frac{\omega_\text{R}}{\omega_\text{AA}},$$

we obtain a quadratic equation for maximum growth rate,

$$0 = \big(\alpha + \beta(1 - x_\text{rP})\big)\, \hat{\mu}^2 + \big(\gamma + x_\text{rP}\big)\, \hat{\mu} - 1 \tag{12}$$

with

$$\begin{aligned} \alpha &= \bar{k}_\text{R}^\text{el} \frac{n_\text{AF}}{k_\text{AF}^\text{cat}} \left(\frac{\omega_\text{AA}}{\omega_\text{R}} \right)^2 \\ \beta &= \bar{k}_\text{R}^\text{el} \left[\frac{n_\text{IC}}{k_\text{IC}^\text{cat}} \frac{\omega_\text{AA}}{\omega_\text{G}} + \left(\frac{n_\text{EAA}}{k_\text{EAA}^\text{cat}} + \frac{n_\text{ENT}}{k_\text{ENT}^\text{cat}} + \frac{n_\text{RNAP}}{\bar{k}_\text{RNAP}^\text{el}} \right) \frac{\omega_\text{AA}}{\omega_\text{NT}} \right] \frac{\omega_\text{AA}}{\omega_\text{R}} \\ \gamma &= \bar{k}_\text{R}^\text{el} \left[\frac{n_\text{IC}}{k_\text{IC}^\text{cat}} \frac{\omega_\text{AA}}{\omega_\text{G}} + \frac{n_\text{EAA}}{k_\text{EAA}^\text{cat}} \right] \frac{\omega_\text{AA}}{\omega_\text{R}}. \end{aligned}$$

Box 2. The determinant method

(In-)homogeneous linear equality and inequality constraints on a vector $x \in \mathbb{R}^n$ can be summarized by matrices $A' \in \mathbb{R}^{m' \times n}$, $A'' \in \mathbb{R}^{m'' \times n}$ and vectors $b' \in \mathbb{R}^{m'}$, $b'' \in \mathbb{R}^{m''}$ as

$$A'x = b', \quad A''x \geq b''.$$

After homogenization, one obtains

$$B'x' = 0, \quad B''x' \geq 0 \quad \text{for} \quad x' = \begin{pmatrix} x \\ 1 \end{pmatrix} \in \mathbb{R}^{n+1},$$

$$\text{where} \quad B' = \left(A', -b'\right) \in \mathbb{R}^{m' \times (n+1)}, \quad B'' = \left(A'', -b''\right) \in \mathbb{R}^{m'' \times (n+1)}.$$

Assume that, for a particular x, all inequality constraints are active, that is, $B''x' = 0$. Then,

$$Bx' = 0,$$

$$\text{where} \quad B = \begin{pmatrix} B' \\ B'' \end{pmatrix} \in \mathbb{R}^{(m'+m'') \times (n+1)}.$$

If B is square (that is, if $m' + m'' = n + 1$), then

$$\det B = 0,$$

that is, its determinant is zero.

In the main text, we consider particular (sub-)sets of constraints on the vector of fluxes v in the form $A'v = b'$, $A''v \geq b''$ and assume that, at maximum growth rate, all constraints are active, and the resulting matrix B is square. We compute its determinant, set it to zero, and determine the maximum growth rate from the resulting (quadratic) equation.

For fixed $x_{\mathrm{rP}} \in [0,1]$, the quadratic equation (12) has one positive solution $\hat{\mu}(x_{\mathrm{rP}})$. To show that it is monotone in x_{rP}, we differentiate (12) and set $\mathrm{d}\hat{\mu}/\mathrm{d}x_{\mathrm{rP}} = 0$. We get

$$0 = -\beta\hat{\mu}^2 + \hat{\mu}$$

which has the positive solution $\hat{\mu} = 1/\beta$. Insertion into (12) yields

$$0 = (\alpha+\beta)\left(\frac{1}{\beta}\right)^2 + \gamma\frac{1}{\beta} - 1 =: \varepsilon,$$

which does not depend on x_{rP}. In fact, if $\varepsilon = 0$, then $\hat{\mu}$ is constant. Otherwise, $\hat{\mu}$ is strictly monotone in x_{rP} (decreasing if $\varepsilon > 0$ and increasing if $\varepsilon < 0$).

For realistic parameters, $\hat{\mu}$ is decreasing (and $\hat{\mu} < 1/\beta$).

Approximation. For realistic parameters, $\alpha \ll \beta \leq 1$, and for all $x_{\mathrm{rP}} \in [0,1]$, we may set $\alpha = 0$ in the quadratic equation (12): For $x_{\mathrm{rP}} \to 0$, obviously $\alpha + (1-x_{\mathrm{rP}})\beta \to \alpha + \beta \approx \beta$. For $x_{\mathrm{rP}} \to 1$, the crucial quantity $4(\alpha + (1-x_{\mathrm{rP}})\beta)/(\gamma + x_{\mathrm{rP}})^2 \to 4\alpha/(1+\gamma)^2 \ll 1$, and the quadratic term can be neglected.

Numerical growth rate maximization

We fix growth rate and solve the system of equations (1) and (2) using efmtool 0.2.0 (***Terzer and Stelling, 2008***) in Python 3.8.13. We use bisection search to find the highest growth rate that still enables a feasible solution.

References

Abeysirigunawardena SC, Kim H, Lai J, Ragunathan K, Rappé MC, Luthey-Schulten Z, Ha T, Woodson SA. Evolution of protein-coupled RNA dynamics during hierarchical assembly of ribosomal complexes. Nature communications. 2017; 8(1):492.

Acca M, Bocchetta M, Ceccarelli E, Creti R, Stetter KO, Cammarano P. Updating Mass and Composition of Archaeal and Bacterial Ribosomes. Archaeal-like Features of Ribosomes from the Deep-Branching Bacterium Aquifex pyrophilus. Systematic and Applied Microbiology. 1993 Feb; 16(4):629–637. https://www.sciencedirect.com/science/article/pii/S0723202011803346, doi: 10.1016/S0723-2020(11)80334-6.

Adilakshmi T, Ramaswamy P, Woodson SA. Protein-independent Folding Pathway of the 16S rRNA 5' Domain. Journal of Molecular Biology. 2005 Aug; 351(3):508–519. https://www.sciencedirect.com/science/article/pii/S0022283605006704, doi: 10.1016/j.jmb.2005.06.020.

Altamura S, Caprini E, Sanchez M, Londei P. Early assembly proteins of the large ribosomal subunit of the thermophilic archaebacterium Sulfolobus. Identification and binding to heterologous rRNA species. Journal of Biological Chemistry. 1991; 266(10):6195–6200.

Bar-Even A, Noor E, Savir Y, Liebermeister W, Davidi D, Tawfik DS, Milo R. The Moderately Efficient Enzyme: Evolutionary and Physicochemical Trends Shaping Enzyme Parameters. Biochemistry. 2011; 50(21):4402–4410. https://doi.org/10.1021/bi2002289, doi: 10.1021/bi2002289, pMID: 21506553.

Bernhardt HS. The RNA world hypothesis: the worst theory of the early evolution of life (except for all the others) a. Biology direct. 2012; 7(1):1–10.

Bernhardt HS, Tate WP. A Ribosome Without RNA. Frontiers in Ecology and Evolution. 2015; 3:129.

Bonven B, Gulløv K. Peptide chain elongation rate and ribosomal activity in Saccharomyces cerevisiae as a function of the growth rate. Molecular and General Genetics MGG. 1979; 170(2):225–230.

Bowman JC, Hud NV, Williams LD. The ribosome challenge to the RNA world. Journal of Molecular Evolution. 2015; 80(3):143–161.

Bremer H, Dennis P. Modulation of chemical composition and other parameters of the cell by growth rate. Escherichia coli and Salmonella: cellular and molecular biology. American Society for Microbiology,. 1996; p. 1553–1568.

Bushhouse DZ, Choi EK, Hertz LM, Lucks JB. How does RNA fold dynamically? Journal of molecular biology. 2022; p. 167665.

Caspi R, Billington R, Fulcher CA, Keseler IM, Kothari A, Krummenacker M, Latendresse M, Midford PE, Ong Q, Ong WK, et al. The MetaCyc database of metabolic pathways and enzymes. Nucleic acids research. 2018; 46(D1):D633–D639.

Cheng ZF, Deutscher MP. Quality control of ribosomal RNA mediated by polynucleotide phosphorylase and RNase R. Proceedings of the National Academy of Sciences. 2003; 100(11):6388–6393. https://www.pnas.org/doi/abs/10.1073/pnas.1231041100, doi: 10.1073/pnas.1231041100.

Choi E, Jeon H, Oh JI, Hwang J. Overexpressed L20 rescues 50S ribosomal subunit assembly defects of bipA-deletion in Escherichia coli. Frontiers in microbiology. 2020; 10:2982.

Dill KA, Ghosh K, Schmit JD. Physical limits of cells and proteomes. Proceedings of the National Academy of Sciences. 2011; 108:17876–17882. doi: 10.1073/pnas.1114477108, publisher: Proceedings of the National Academy of Sciences.

Dos Santos RF, Quendera AP, Boavida S, Seixas AF, Arraiano CM, Andrade JM. Major 3'–5' exoribonucleases in the metabolism of coding and non-coding RNA. Progress in molecular biology and translational science. 2018; 159:101–155.

Fazal FM, Koslover DJ, Luisi BF, Block SM. Direct observation of processive exoribonuclease motion using optical tweezers. Proceedings of the National Academy of Sciences. 2015; 112(49):15101–15106.

French SL, Santangelo TJ, Beyer AL, Reeve JN. Transcription and Translation are Coupled in Archaea. Molecular Biology and Evolution. 2007 Jan; 24(4):893–895. https://academic.oup.com/mbe/article-lookup/doi/10.1093/molbev/msm007, doi: 10.1093/molbev/msm007.

Gausing K. Regulation of ribosome production in Escherichia coli: synthesis and stability of ribosomal RNA and of ribosomal protein messenger RNA at different growth rates. Journal of molecular biology. 1977; 115(3):335–354.

Gehring AM, Santangelo TJ. Archaeal RNA polymerase arrests transcription at DNA lesions. Transcription. 2017 Jun; 8(5):288–296. https://www.ncbi.nlm.nih.gov/pmc/articles/PMC5703245/, doi: 10.1080/21541264.2017.1324941.

Goelzer A, Muntel J, Chubukov V, Jules M, Prestel E, Nölker R, Mariadassou M, Aymerich S, Hecker M, Noirot P, et al. Quantitative prediction of genome-wide resource allocation in bacteria. Metabolic engineering. 2015; 32:232–243.

Greber BJ, Boehringer D, Godinic-Mikulcic V, Crnkovic A, Ibba M, Weygand-Durasevic I, Ban N. Cryo-EM structure of the archaeal 50S ribosomal subunit in complex with initiation factor 6 and implications for ribosome evolution. Journal of molecular biology. 2012; 418(3-4):145–160.

Hartl FU, Hayer-Hartl M. Converging concepts of protein folding in vitro and in vivo. Nature structural & molecular biology. 2009; 16(6):574–581.

Hu XP, Dourado H, Schubert P, Lercher MJ. The protein translation machinery is expressed for maximal efficiency in Escherichia coli. Nature communications. 2020; 11(1):5260.

Hyeon C, Thirumalai D. Chain length determines the folding rates of RNA. Biophysical journal. 2012; 102(3):L11–L13.

Jain C. Role of ribosome assembly in Escherichia coli ribosomal RNA degradation. Nucleic acids research. 2018; 46(20):11048–11060.

Jeffares DC, Poole AM, Penny D. Relics from the RNA world. Journal of molecular evolution. 1998; 46:18–36.

Jun SH, Hyun J, Cha JS, Kim H, Bartlett MS, Cho HS, Murakami KS. Direct binding of TFEα opens DNA binding cleft of RNA polymerase. Nature communications. 2020; 11(1):1–12.

Kisly I, Tamm T. Archaea/eukaryote-specific ribosomal proteins-guardians of a complex structure. Computational and Structural Biotechnology Journal. 2023; .

Klumpp S. Speed Limit for Cell Growth. Physics. 2020; 13:108. doi: 10.1103/PhysRevLett.125.028103.

Kostinski S, Reuveni S. Ribosome Composition Maximizes Cellular Growth Rates in E. coli. Physical Review Letters. 2020; 125(2):028103. doi: 10.1103/PhysRevLett.125.028103.

513 **Kurland CG**. Molecular characterization of ribonucleic acid from *Escherichia coli* ribosomes: I. Isolation and
514 molecular weights. Journal of Molecular Biology. 1960; 2(2):83–91.

515 **K Lenz T**, M Norris A, V Hud N, Dean Williams L. Protein-free ribosomal RNA folds to a near-native state in the
516 presence of Mg 2+. RSC Advances. 2017; 7(86):54674–54681. https://pubs.rsc.org/en/content/articlelanding/
517 2017/ra/c7ra08696b, doi: 10.1039/C7RA08696B, zSCC: NoCitationData[s0].

518 **Londei P**, Ferreira-Cerca S. Ribosome biogenesis in archaea. Frontiers in Microbiology. 2021; 12:1476.

519 **Londei P**, Teuudò J, Acca M, Cammarano P, Amils R. Total reconstitation of active large ribosomal subunlts of
520 the tbermoaddophllk arcfaaebacterium Sulfolobus solfataricus. Nucleic acids research. 1986; 14(5):2269–
521 2285.

522 **Long CP**, Gonzalez JE, Cipolla RM, Antoniewicz MR. Metabolism of the fast-growing bacterium Vibrio natriegens
523 elucidated by 13C metabolic flux analysis. Metabolic engineering. 2017; 44:191–197.

524 **Martick M**, Scott WG. Tertiary contacts distant from the active site prime a ribozyme for catalysis. Cell. 2006;
525 126(2):309–320.

526 **Melnikov S**, Ben-Shem A, Garreau de Loubresse N, Jenner L, Yusupova G, Yusupov M. One core, two shells:
527 bacterial and eukaryotic ribosomes. Nature Structural & Molecular Biology. 2012 Jun; 19(6):560–567. https:
528 //www.nature.com/articles/nsmb.2313, doi: 10.1038/nsmb.2313.

529 **Melnikov S**, Manakongtreecheep K, Söll D. Revising the structural diversity of ribosomal proteins across the
530 three domains of life. Molecular Biology and Evolution. 2018; 35(7):1588–1598.

531 **Milo R**, Jorgensen P, Moran U, Weber G, Springer M. BioNumbers—the database of key numbers in molecular
532 and cell biology. Nucleic Acids Research. 2009 10; 38(suppl_1):D750–D753. https://doi.org/10.1093/nar/
533 gkp889, doi: 10.1093/nar/gkp889.

534 **Milo R**, Phillips R. Cell biology by the numbers. Garland Science; 2015.

535 **Moore PB**. In Which the Deity Attempts To Make a Ribose-Free Ribosome. Biochemistry. 2019; 58(6):431–432.
536 https://doi.org/10.1021/acs.biochem.8b01191, doi: 10.1021/acs.biochem.8b01191.

537 **Müller S**, Széliová D, Zanghellini J. Elementary vectors and autocatalytic sets for resource allocation in next-
538 generation models of cellular growth. PLoS computational biology. 2022; 18(2):e1009843.

539 **Petrov AS**, Gulen B, Norris AM, Kovacs NA, Bernier CR, Lanier KA, Fox GE, Harvey SC, Wartell RM, Hud NV, et al.
540 History of the ribosome and the origin of translation. Proceedings of the National Academy of Sciences.
541 2015; 112(50):15396–15401.

542 **Proshkin S**, Rahmouni AR, Mironov A, Nudler E. Cooperation Between Translating Ribosomes and RNA Poly-
543 merase in Transcription Elongation. Science. 2010 Apr; 328(5977):504–508. https://www.science.org/doi/10.
544 1126/science.1184939, doi: 10.1126/science.1184939.

545 **Ramrath DJ**, Niemann M, Leibundgut M, Bieri P, Prange C, Horn EK, Leitner A, Boehringer D, Schneider A, Ban
546 N. Evolutionary shift toward protein-based architecture in trypanosomal mitochondrial ribosomes. Science.
547 2018; 362(6413):eaau7735.

548 **Reuveni S**, Ehrenberg M, Paulsson J. Ribosomes are optimized for autocatalytic production. Nature. 2017;
549 547(7663):293–297.

550 **Rodgers ML**, Woodson SA. Transcription Increases the Cooperativity of Ribonucleoprotein Assembly. Cell.
551 2019; 179(6):1370–1381.e12. https://www.sciencedirect.com/science/article/pii/S0092867419312280, doi:
552 https://doi.org/10.1016/j.cell.2019.11.007.

553 **Rodgers ML**, Woodson SA. A roadmap for rRNA folding and assembly during transcription. Trends in Biochem-
554 ical Sciences. 2021; 46(11):889–901.

555 **Rohatgi A**, Webplotdigitizer: Version 4.6; 2022. https://automeris.io/WebPlotDigitizer, last accessed on 2017-
556 11-30.

557 **Scott M**, Gunderson CW, Mateescu EM, Zhang Z, Hwa T. Interdependence of cell growth and gene expression:
558 origins and consequences. Science. 2010; 330(6007):1099–1102.

559 **Shajani Z**, Sykes MT, Williamson JR. Assembly of Bacterial Ribosomes. Annual Review of Biochemistry.
560 2011 Jul; 80(1):501–526. https://www.annualreviews.org/doi/10.1146/annurev-biochem-062608-160432, doi:
561 10.1146/annurev-biochem-062608-160432.

562 **Shore D**, Albert B. Ribosome biogenesis and the cellular energy economy. Current Biology. 2022; 32(12):R611–
563 R617.

564 **Sutherland C**, Murakami KS. An introduction to the structure and function of the catalytic core enzyme of
565 Escherichia coli RNA polymerase. EcoSal Plus. 2018; 8(1).

566 **Terzer M**, Stelling J. Large-scale computation of elementary flux modes with bit pattern trees. Bioinformatics.
567 2008; 24(19):2229–2235.

568 **Tirumalai MR**, Rivas M, Tran Q, Fox GE. The peptidyl transferase center: a window to the past. Microbiology
569 and Molecular Biology Reviews. 2021; 85(4):e00104–21.

570 **Verschoor A**, Warner JR, Srivastava S, Grassucci RA, Frank J. Three-dimensional structure of the yeast ribosome.
571 Nucleic Acids Research. 1998 Jan; 26(2):655–661. https://academic.oup.com/nar/article-lookup/doi/10.1093/
572 nar/26.2.655, doi: 10.1093/nar/26.2.655.

573 **Wilson DN**, Cate JHD. The Structure and Function of the Eukaryotic Ribosome. Cold Spring Harbor Perspectives
574 in Biology. 2012 May; 4(5):a011536. http://cshperspectives.cshlp.org/content/4/5/a011536, doi: 10.1101/csh-
575 perspect.a011536.

576 **Woellhaf MW**, Hansen KG, Garth C, Herrmann JM. Import of ribosomal proteins into yeast mitochondria. Bio-
577 chemistry and Cell Biology. 2014; 92(6):489–498.

Appendix 1

Supplementary figures

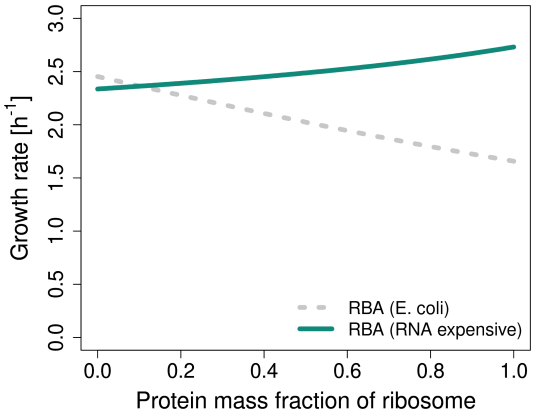

Appendix 1 Figure 1. RBA with realistic parameters for glucose minimal medium from ***Table 2*** (grey curve) vs. RBA with parameters that make RNA more expensive than proteins ($\bar{k}^{el}_{RNAP} = 8.5\,NT\,s^{-1}$, $\bar{k}^{el}_{R} = 63\,AA\,s^{-1}$, $n_{RNAP} = 52470$; green curve).

(a) No cooperativity: $k^{deg}(x_{rP}) = k^{deg}_{max}$

(b) Weak cooperativity: $k^{deg}(x_{rP}) = k^{deg}_{max}(1 - \frac{x^2_{rP}}{K^2 + x^2_{rP}})$

(c) Strong cooperativity: $k^{deg}(x_{rP}) = k^{deg}_{max}(1 - \frac{x^6_{rP}}{K^6 + x^6_{rP}})$

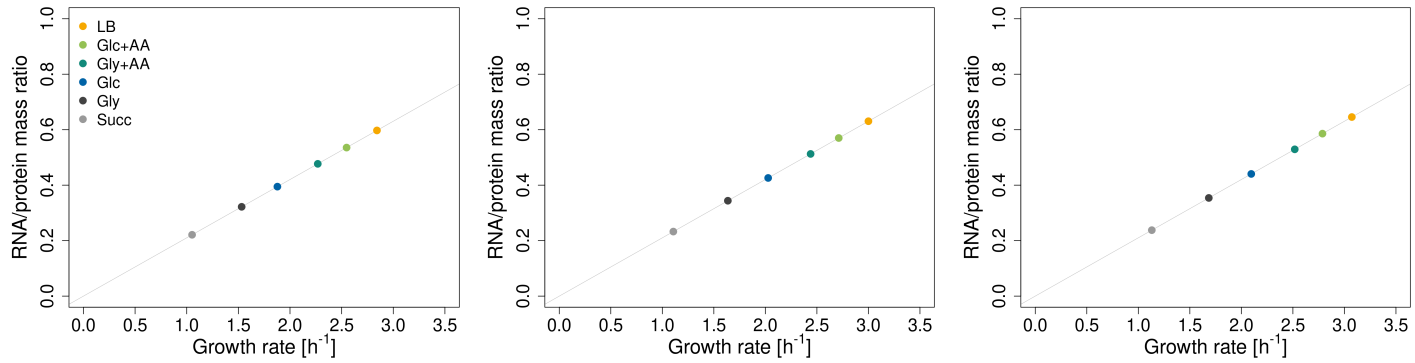

Appendix 1 Figure 2. Our model recapitulates linear relationship of RNA:protein mass ratio and growth rate for all three forms of rRNA degradation function.

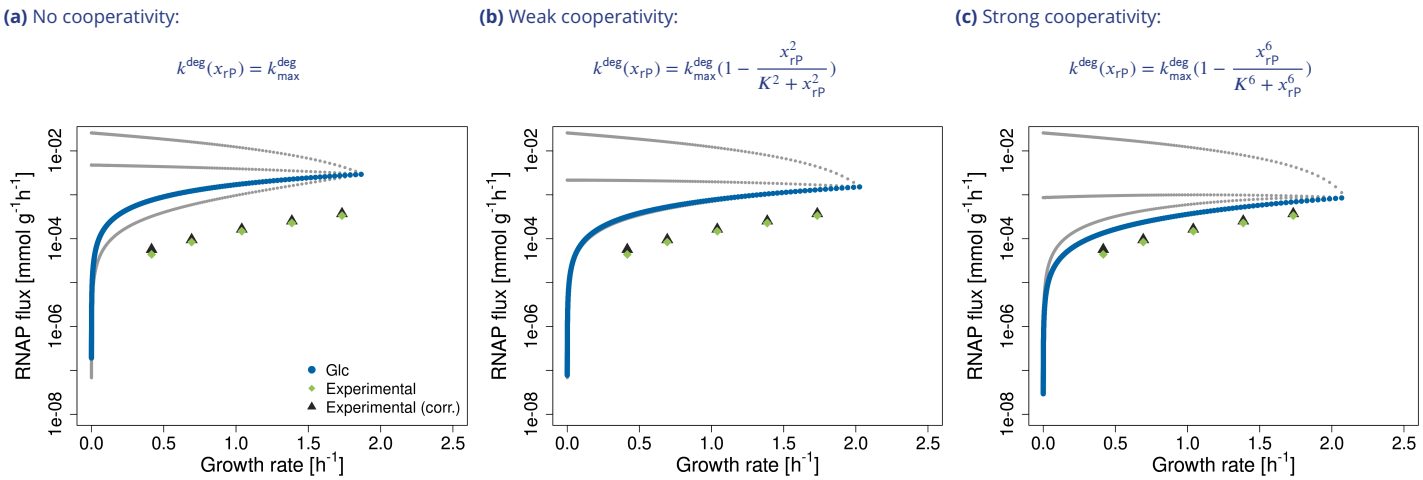

Appendix 1 Figure 3. RNAP fluxes as functions of growth rate for glucose minimal medium. Gray and blue lines are simulations. Light green diamonds are experimental data from ***Bremer and Dennis*** (***1996***), and black triangles are data from ***Bremer and Dennis*** (***1996***) corrected for rRNA degradation (***Gausing, 1977***). Data were converted to $\mathrm{mmol\,g^{-1}\,h^{-1}}$ with *E. coli* dry masses from ***Milo and Phillips*** (***2015***).

Unlike in the base model (***Figure 2b***), we observe four instead of three EGVs. The top gray trajectory represents solutions where RNase activity is higher than the enforced minimum given by Eqn. (5), which leads to increased RNAP flux. The middle gray trajectory are solutions where ribosomes accumulate in excess of what is needed for growth. This also increases rRNA degradation via equation (5) and therefore RNAP fluxes. Finally, the bottom gray solutions accumulate rRNA. Blue corresponds to EGVs where rRNA and ribosomes are not accumulating and rRNA is not degraded in excess, that is, constraints "rRNA", "cap R" and "min deg" in ***Table 1*** are fulfilled with equality.

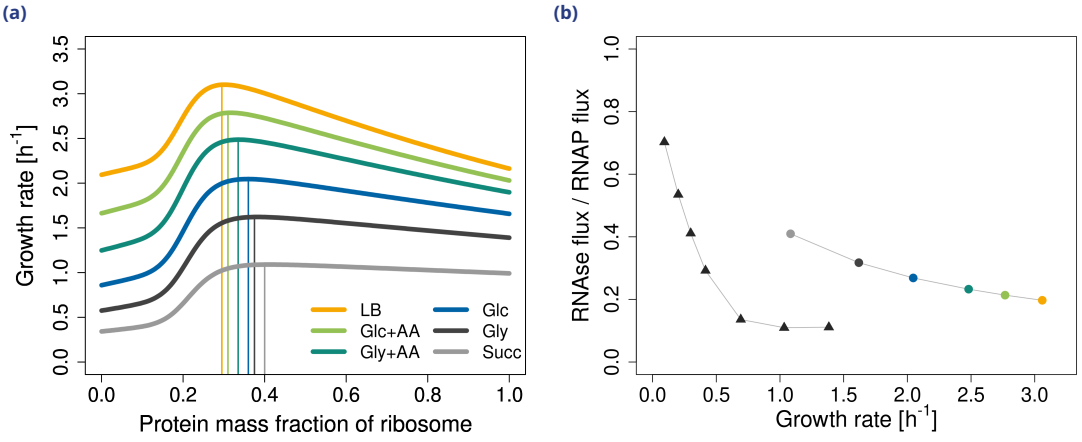

Appendix 1 Figure 4. Accounting for RNAP allocation improves predictions of RNase fluxes. **(a)** Maximum growth rate for *E. coli* in six different conditions (see ***Table 2***). **b** Ratio of RNA degradation to RNA transcription (RNAse flux/RNAP flux) The circles are the predicted ratios of RNAse fluxes to RNAP fluxes at different conditions. The triangles represent experimental data from ***Gausing*** (***1977***) (extracted from the original plot with WebPlotDigitizer (***Rohatgi, 2022***)).